IMPACT OF IL-4 RECEPTOR INHIBITION ON MORBIDITY RELATED TO H1N1 INFECTION IN A MURINE MODEL OF ALLERGIC ASTHMA

by

Kimeya Shahangian

B.Sc., The University of British Columbia, 2016

A THESIS SUBMITTED IN PARTIAL FULFILLMENT OF

THE REQUIREMENTS FOR THE DEGREE OF

MASTER OF SCIENCE

in

THE FACULTY OF GRADUATE AND POSTDOCTORAL STUDIES

(Experimental Medicine)

THE UNIVERSITY OF BRITISH COLUMBIA

(Vancouver)

January 2019

The following individuals certify that they have read, and recommend to the Faculty of Graduate and Postdoctoral Studies for acceptance, a thesis/dissertation entitled:

The Role of IL-4 Receptor Inhibition on Morbidity Related to H1N1 Infection in a Murine Model of Allergic Asthma

submitted by Kimeya Shahangian in partial fulfillment of the requirements for

the degree of Master of Science

in Experimental Medicine

Examining Committee:

Dr. Don Sin
Co-supervisor

Dr. Kelly McNagny
Co-supervisor

Dr. Paul Man
Supervisory Committee Member

Dr. Fumio Takei
Additional Examiner

Abstract

The 2009 H1N1 pandemic observed a large percentage of morbidity and mortality attributed to individuals with asthma. However, a consistent lack of preventative and therapeutic interventions failed to protect this vulnerable population. Vaccines are the most effective method of prevention, yet they take at least 6 months to be developed following outbreak of a pandemic strain. Meanwhile, antiviral drugs are the sole method of treatment, yet their clinical use can be restricted due to drug resistance. Hence, pre-planning is required to develop interventions that could protect the vulnerable asthmatic population prior to the occurrence of the next influenza pandemic.

A Th_2-skewed inflammatory response has been implicated in the development of some of the characteristics of asthma, whereby IL-4, IL-5, and IL-13 signaling promotes airway eosinophilia and lung remodeling. IL-4 and IL-13 signal through the common alpha subunit of the IL-4 receptor (IL-4Rα) to induce their effector function. Clinical trials have found the blockade of IL-4Rα to be highly effective at reducing the rate of asthmatic exacerbations. However, it has yet to be determined whether IL-4Rα blockade could protect against pandemic H1N1 (pH1N1)-mediated morbidity. We hypothesized that IL-4Rα blockade could be used as a treatment method in an established pH1N1 infection, and as a prevention method prior to and after pH1N1 infection, in a murine model of allergic asthma.

Our findings indicate that both the treatment and prevention strategies of IL-4Rα blockade induce a significant reduction in pH1N1-mediated weight-loss in house dust-mite (HDM) sensitized mice. Furthermore, reduced weight-loss was associated with a significant reduction in the number of viral copies, indicating improved viral control. Lastly, IL-4Rα

preventative intervention induced a significant reduction in the level of airway goblet cell metaplasia and the percentage of eosinophils in Bronchoalveolar Lavage (BAL), pointing to lessened allergic manifestations.

While influenza pandemics are rare, they have a devastating effect on the most vulnerable individuals suffering from asthma. Hence, developing pharmaceutical interventions that could benefit this population are of outmost value. Findings from our study could be considered as a strategy to reduce the risk of complications in asthmatic individuals during an H1N1 influenza pandemic.

Lay Summary

During the 2009 H1N1 pandemic, a large percentage of individuals who experienced morbidity and mortality were asthmatics. However, a lack of prevention and treatment strategies to protect this vulnerable population prevailed. Dupilumab is a drug that has been shown to reduce some of the asthma-associated immune responses in humans by blocking the function of a protein named IL-4Rα. However, it is unclear whether IL-4Rα blockade could reduce pandemic H1N1 (pH1N1)-associated morbidity and mortality in the asthmatic population. Using a mouse model of allergic asthma, we investigated the role of IL-4Rα blockade during pH1N1 infection. We found that allergic mice infected with pH1N1 experienced less weight loss and had lower viral burden when IL-4Rα was blocked. Findings from this study could be utilized in the clinical setting to protect individuals with asthma when the next influenza pandemic occurs.

Preface

Work presented in this dissertation was conducted at the Centre for Health Lung Innovation (St. Paul's Hospital) at the University of British Columbia, and the Faculty of Health Sciences at Simon Fraser University. All experiments presented in this thesis were performed in accordance with the UBC Animal Care Committee guidelines (certificate number A16-0331), and the Biosafety Committee guidelines (certificate number B17-0007).

Data presented in chapter 2 were primarily designed and conducted by D. Ngan and Y. Oh. I was responsible for the design, execution, and data analysis of the work presented in chapters 3 and 4. D. Ngan, Dr. T. Wada, and S. Tam provided technical assistance in animal sample collection. D. Ngan performed qPCR experiments for viral titre, and ELISA experiments for pH1N1-specific IgG. A. Samra performed histological sectioning and staining. Dr. M. Niikura provided valuable reagents. Drs. K. McNagny, P. Man, and J. Hirota provided intellectual content and aided in experimental design. Dr. D. Sin supervised the project and directed the research.

Table of Contents

List of Figures

List of Abbreviations

AEC	Airway Epithelial cell
AHR	Airway Hyper-responsiveness
ANOVA	Analysis of Variance
BALF	Bronchoalveolar Lavage Fluid
CAF	Chorioallantoic Fluid
CDC	Centers for Disease Control and Prevention
cRNA	complimentary Ribonucleic Acid
CTL	Cytotoxic T Cell
DC	Dendritic Cell
EID_{50}	fifty percent Embryo Infectious Dose
ER	Endoplasmic Reticulum
FasL	Fas Ligand
FeNO	Fractional exhaled Nitric Oxide
FEV_1	Forced Expiratory Volume in 1 second
GPCR	G Protein-coupled Receptor
HA	Hemagglutinin
HDM	House Dust-mite extract
IAV	Influenza A Virus
ICU	Intensive Care Unit
IFN	Interferon

IL	Interleukin
IL-4Ra	The alpha chain of IL-4 Receptor
ILC2	Innate Lymphoid Cell type 2
IN	Intranasal
iNOS	inducible Nitric Oxide Synthase
IP	Intraperitoneal
IRF	Interferon Regulatory Factor
IRS-2	Insulin Receptor Substrate 2
ISG	Interferon Stimulated Gene
JAK	Janus Kinase
M1	Matrix protein 1
M2	Matrix protein 2
MHC	Major Histocompatibility Complex
mAB	monoclonal Antibody
MR	Mannose Receptor
mRNA	messenger Ribonucleic Acid
MxA	Myxovirus resistance gene A
NA	Neuraminidase
NEP	Nuclear Export Protein
NF-KB	Nuclear Factor Kappa-light-chain-enhancer of activated B cells
NK	Natural Killer cell
NLRP3	NOD-like Receptor Protein 3
NPI	Non-pharmaceutical Interventions

OD	Optical Density
OVA	Ovalbumin
p.i.	post-infection
PAMP	Pathogen-associated Molecular Patterns
PAR-2	Protease-activated Receptor 2
PAS	Periodic Acid-Schiff
PBS	Phosphate-buffered Saline
PC20	Provocative Concentration to cause a 20% decrease in FEV_1
PEF	Peak Expiratory Flow
pH1N1	pandemic H1N1
PI3K	Phosphoinositide-3-kinase
PRR	Pattern Recognition Receptor
RIG-I	Retinoic acid-inducible Gene I
ROS	Reactive Oxygen Species
RSV	Respiratory Syncytial Virus
RV	Rhinovirus
SH2	Src Homology 2 domain
Th_1	T helper cell type 1
Th_2	T helper cell type 2
TLR	Toll-like Receptor
TNF-α	Tumour Necrosis Factor alpha
TRAIL	TNF-related Apoptosis-inducing Ligand
TRIM	Tripartite Motif-containing protein

TSLP	Thymic Stromal Lymphopoietin
TYK2	Tyrosine Kinase 2
vRNP	viral Ribonucleoprotein
WHO	World Health Organization
ZAP	Zinc-finger Antiviral Protein

Acknowledgements

First and foremost, thank you to my supervisor, Dr. Don Sin, for your mentorship and for giving me the opportunity to learn and grow through this journey. I would also like to thank my committee members, Dr. Kelly McNagny and Dr. Paul Man for your time and scientific guidance. My sincere gratitude goes to Dr. Jeremy Hirota and Dr. Masahiro Niikura for providing insightful knowledge and suggestions to drive this project forward.

To all current and past Sin lab members, thank you for your help and support both in and out of the lab. In particular, thanks to David Ngan and Yeni Oh for pioneering this project and providing valuable technical support and training along the way. Thank you Dr. David Jaw, Dr. Takeyuki Wada, Dr. Anthony Tam, and Dr. Chung Cheung for your guidance and assistance. I would also like to thank my fellow lab mates and friends, Minhee Jin, Basak Sahin, Julia Yang, Nancy Yang, and Dr. Fernando Studart for making this such a joyful experience.

Thank you to all the amazing staff at the Centre for Heart Lung Innovation for your assistance. In particular, I'd like to thank Tatjana Bozin, Claire Smits, and Lubos Bohunek at the GEM facility, and Amrit Samra at the histology facility for your expertise and technical support.

Last but not least, thank you to my family for your unwavering support. To my husband Reza, thank you for always believing in me and supporting me throughout this journey.

Chapter 1: Introduction

1.1 Influenza A Virus – From Seasonal Flu to a Pandemic

Each year, the seasonal influenza virus infects 10-20% of the world's population, resulting in 3-5 million hospitalizations [1]. In Canada, there may be up to 30,000 laboratory-confirmed cases and an estimated annual death toll of over 5000 individuals within one influenza season [2]. In the United States, direct medical costs and loss of productivity from each influenza season result in over $87 billion in total annual economic burden [3]. While people of all ages can be infected, infection rates are generally highest in children under 5 and in adults above 65, and the most common comorbidities consist of cardiac and respiratory conditions [2]. The influenza A virus (IAV) typically replicates in the upper respiratory tract, and more severe infections are associated with replication within the lower respiratory tract. IAV infection can cause disease lasting up to 10 days, with a peak in viral replication occurring 2 days after infection. Symptoms include fever, cough, and nasal mucous discharge [4].

Although IAV can cause disease in a variety of animals, it is most commonly observed in humans, birds (avian), pigs (swine) and horses (equine) [5]. Avian IAV generally replicates in the small intestine and is shed in the feces of birds, while swine, equine, and human IAV replicate in the airways and are spread via respiratory droplets [5,6]. Moreover, human IAV has a different receptor-binding specificity than IAV from other origins; although sialic acid bound to a galactose chain is always used as a receptor, human IAV preferentially binds an α2-6 linkage, while avian IAV binds an α2-3 linkage [7]. Therefore, while IAV of different origins have been sporadically reported in humans, human-to-human transmission and the pandemic potential of influenza depend on the virus' ability to bind an α2-6 linkage.

IAV is classified into different subtypes based on its envelope glycoproteins, namely hemagglutinin (HA) and neuraminidase (NA). In order to evade the host's acquired immunity, IAV undergoes frequent random mutations in the HA and NA genes to create a diffuse cloud of antigenic receptors. The term "Antigenic Drift" is used to refer to the gradual accumulation of mutations in HA and NA proteins of IAV to confer pathogenic capacity during each seasonal flu cycle [8]. These mutations are generally caused by a few amino acid substitutions adjacent to the receptor binding domain in the HA protein [9]. In contrast, "Antigenic Shift" refers to drastic changes in the antigenicity of the HA protein, and has been associated with the occurrence of pandemics. These pandemic strains generally arise through genetic re-assortment between human and avian viruses [10]. Due to their ability to express both the α2-6 and the α2-3 linkages, pigs can act as a "mixing vessel" for the generation of a re-assorted unique pandemic strain. Swine influenza can also contribute to the re-assortment process, creating a triple-re-assorted IAV such as the one that caused the 2009 H1N1 pandemic [11].

The earliest, and by far the deadliest recorded incidence of an IAV pandemic was the 1918 Spanish flu, which killed between 20-50 million people worldwide (an estimated 2.5% of the entire population). Genetic analysis performed on viral RNA recovered from lung tissue of victims indicate that the Spanish flu was an H1N1 subtype from an avian origin [12]. Since then, four other influenza pandemics have occurred, namely the 1957 Asian flu (H2N2 subtype, avian origin), the 1968 Hong Kong flu (H3N2 subtype, avian origin), the 1977 Russian flu (H1N1 subtype, thought to have been caused by a laboratory-maintained virus), and the 2009 swine flu (H1N1 subtype, genes from avian, contemporary human H3N2, and swine viruses) [5,13-15]. Although influenza pandemics are not common, historical records indicate that they can occur every 10-40 years.

While several influenza pandemics have swept the world in the past, there are a limited number of prevention and treatment strategies in place that can be quickly and effectively implemented. Vaccines remain the most effective method of prevention. However, development of vaccines and the implementation of vaccination programs take at least 6 months from the time that a new pandemic strain is identified [16]. Hence, the only prevention strategy available to the population during the 6 month waiting period are non-pharmaceutical interventions (NPIs). NPIs consist of community mitigation guidelines that include pre-pandemic planning at multiple levels. It encompasses personal protective measures (e.g. quarantine of exposed family members, use of face masks), drastic and seldom used community measures (e.g. school closures, cancelling of mass gatherings), as well as environmental measures (e.g. routine cleaning of frequently used surfaces) [17,18]. While the main focus of NPIs are to delay spread and reduce the impact of the influenza pandemic, computational models have demonstrated that they decrease the mean attack rate (percentage of the population that can become infected over the course of the pandemic) by only 2% in a severe pandemic scenario [19]. Hence, a more effective prevention strategy needs to be developed to limit influenza spread and the associated health complications in order to prepare for future pandemics.

There are currently two classes of general antiviral drugs used to treat IAV infections, namely adamantanes (e.g. amantadine and rimantadine) and neuraminidase inhibitors (e.g. oseltamivir and zanamivir) [20]. In the case of the 2009 pandemic strain (pH1N1), the virus had developed a mutation that made it resistant to adamantanes, leaving neuraminidase inhibitors as the only available treatment option for infected individuals [21]. Oseltamivir proved to be highly effective against pH1N1, and allowed faster resolution of symptoms as well as a more rapid clearance of viral shedding in hospitalized patients [22,23]. However, the efficacy of oseltamivir

treatment significantly decreases with a delay in seeking treatment [23,24]. Furthermore, up to 3% of pH1N1 patients treated with oseltamivir displayed resistance, which studies have reported to occur within 48 hours of treatment [25,26]. Hence, effective and efficient treatment strategies that are not susceptible to viral resistance are desperately needed for future pandemics.

1.2 IAV Structure and Lifecycle

IAV belongs to the *Orthomyxoviridae* family of viruses, and is classified based on its envelope glycoproteins HA and NA [27]. It has a single stranded RNA genome, segmented into 8 viral Nucleoproteins (vRNPs). The segmented nature of its genome allows frequent re-assortment with other IAVs when two viruses infect the same cell [10].

Human IAV mainly infects the epithelial cells of the upper respiratory tract that express sialic acid connected via an α2-6 linkage to an oligosaccharide chain. The HA protein preferentially binds to this receptor, triggering endocytosis of the virus [27]. Upon internalization, acidification of the endosome causes a conformational change in HA [28]. This mediates the activation of the Matrix Protein 2 (M2), a hydrogen ion channel that further lowers the pH within the endosome [29]. Acidic pH results in the fusion of the viral envelope with the endosome membrane, and release of vRNPs into the cytoplasm [30]. vRNPs are then directed to the nucleus via nuclear localization signals, and subsequently transported via nuclear pores [31]. Within the nucleus, the viral RNA-dependent RNA polymerase has the dual function of performing RNA transcription to create messenger RNA (mRNA), as well as RNA replication to create viral complementary RNA (cRNA) [32]. Host cellular mechanisms are subsequently used to transport mRNA into the cytoplasm, where translation is performed by host ribosomes [10,32]. In contrast, viral cRNA is used as a template to create negative-sense genomic RNA,

which is subsequently bound with Matrix protein 1 (M1) and the Nuclear Export Protein (NEP) to be transported out of the nucleus [32,33]. After leaving the nucleus, vRNPs use host factors and microtubules to traffic to the apical side of the plasma membrane [34-36]. M1 has been shown to be important for virion assembly through the recruitment of viral and host components, while NA is required for viral budding and the release of the newly formed virions by facilitating sialic acid cleavage on the host membrane [37,38].

1.3 Host Responses to IAV

Upon IAV infection, the host launches a rapid yet non-specific innate immune response to limit viral replication. The virus is detected by the host through the binding of Pathogen Associated Molecular Patterns (PAMPs) to one of two Pathogen Recognition Receptors (PRRs) present on innate immune cells (Dendritic cells (DCs) and macrophages), namely Toll-like Receptor (TLR)-7 and Retinoic acid Inducible Gene I (RIG-I) [39]. RIG-I is a cytosolic sensor, and recognizes 5' triphosphates on single stranded viral RNA, leading to the activation of Interferon Regulatory Factor (IRF)-3 and Nuclear Factor Kappa-light-chain enhancer of activated B cells (NF-KB) [39,40]. On the other hand, TLR-7 recognizes single stranded viruses that are taken up by the endosome, and leads to the activation of IRF-7 and NF-KB [39,41]. As transcription factors, IRF-3 and 7 translocate to the nucleus and induce the production of type I Interferons (IFNs), while NF-KB induces the production of a variety of pro-inflammatory cytokines [39]. Furthermore, RIG-I and TLR-7 are both involved in the activation of the Nod-like Receptor Protein 3 (NLRP3) inflammasome, leading to the cleavage and activation of pro-Interleukin(IL)-1β and pro-IL-18, thus resulting in the amplification of a pro-inflammatory immune response [42,43].

The production of type I IFNs, namely IFN-α and IFN-β, has been demonstrated to be effective in inhibiting viral replication through the induction of Interferon Stimulated Genes (ISGs) [44]. ISGs are a set of proteins that can induce an antiviral state through targeting different steps of the IAV lifecycle. For example, ISGs can inhibit viral entry by converting cholesterol on the cell membrane to 25-hydroxycholesterol (Cholesterol-25-hydroxylase), enhance RIG-I activity and virus recognition (Tripartite motif-containing protein (TRIM)-25), inhibit viral entry into the nucleus (Myxovirus resistance gene A(MxA)), inhibit viral replication by blocking IAV polymerase activity (TRIM32), reduce viral mRNA expression and therefore protein production (Zinc-finger antiviral proteins (ZAPs)), and prevent viral release by perturbing lipid rafts (Virus inhibitory protein (Viperin)) [45-50]. Type I IFNs and subsequent ISG expression are thus important in establishing an antiviral state during IAV infection.

Several innate cells have important roles in the innate immune response during the first few days of infection. Infected epithelial cells produce the chemokine CCL2, which recruits macrophages to the site of infection, resulting in the phagocytosis of infected and apoptotic cells [51,52]. Studies have demonstrated that the depletion of alveolar macrophages results in uncontrolled viral titres and increased mortality in mice, pointing to the importance of these cells in IAV control [53]. Macrophages and Natural Killer (NK) cells are also the primary source of IFN-γ, an important antiviral cytokine, during the first 3 days of infection [43]. Furthermore, the NKp46 receptor on NK cells can recognize and bind to the HA protein of IAV, mediating direct lysis of the virus [54].

DCs are important antigen presenting cells that act as the mediator of innate to adaptive immunity. DCs that are infected by the virus can induce the proteasomal degradation of viral proteins in the cytosol. Viral proteins are then transported to the Endoplasmic Reticulum (ER),

where they are attached to the Major Histocompatibility Complex (MHC)-I, and subsequently transported to the cell surface for representation to T lymphocytes [39,55]. DCs are also constantly inspecting the lung for pathogens, and are able to phagocytose the virus upon identification. Phagocytosed viral proteins are degraded in the endosome, where they are associated with MHC-II, and subsequently moved to the cell surface [39]. Following antigen processing, DCs migrate to the mediastinal lymph node via CCR7 signaling, where they present IAV-derived antigens to $CD4^+$ (via MHC-II-antigen complex) and $CD8^+$ (via MHC-I-antigen complex) naïve or memory T cells [39,56].

Engagement with the MHC-I-antigen complex on DCs and co-stimulatory cytokines such as IFN-γ and IL-2 can induce the proliferation and differentiation of $CD8^+$ T cells into Cytotoxic T Lymphocytes (CTLs) [57,58]. CTLs directly "kill" infected cells through two different mechanisms. Firstly, CTLs produce cytotoxic granules such as perforin and granzyme. Perforin is able to form pores on the cell membrane, allowing passive diffusion of granzyme into the target cell. Granzyme subsequently cleaves viral and host proteins important for viral life cycle [59,60]. Furthermore, CTLs can produce Tumour Necrosis Factor-α (TNF-α), Fas Ligand (FasL), and TNF-related Apoptosis-inducing Ligand (TRAIL). The signaling of these cytokines can induce apoptosis in the infected cells [39,59,61].

Alternatively, DCs presenting viral antigens on MHC-II can produce IL-12, which induces the differentiation of $CD4^+$ T cells into T helper type 1 (Th_1) cells [62]. Th_1 cells are able to provide "help" to other immune cells through the production of IFN-γ and TNF-α to induce IAV protection [63,64]. As an important antiviral cytokine, IFN-γ can upregulate the cell surface expression of MHC-I, thus increasing the potential for cytotoxic T cell activation and further viral clearance [65]. Furthermore, IFN-γ activates macrophage effector function by increasing

pinocytosis and receptor-mediated phagocytosis, and upregulates the expression of the inducible Nitric Oxide Synthase (iNOS) and Reactive Oxygen Species (ROS) production to increase the ability of macrophages to kill viruses [65-67]. Lastly, IFN-γ induces the differentiation of $CD4^+$ T cells towards a Th_1 phenotype, resulting in a positive-feedback loop that can effectively eliminate the virus [65].

1.4 The 2009 H1N1 Pandemic

A novel strain of pandemic influenza (pH1N1) was first identified in Mexico in March 2009, and quickly swept the globe owing in part to modern advancements in transportation. Over 26,000 cases were reported only three months after its initial identification, leading the World Health Organization (WHO) to announce a phase 6 pandemic (on the 6-point scale influenza alert system) and a public health emergency on June 11, 2009 [68,69]. Worldwide, the pandemic caused over 18,500 laboratory confirmed deaths. Considering the lack of healthcare facilities and thus fewer cases tested in developing countries, this number is believed to be a gross underestimation of the true impact of the pandemic. Using computational models, Dawood et al. estimated the true number of pH1N1-mediated deaths to lie between 151,700–575,500 individuals, with 51% of mortality attributed to countries in South-East Asia and Africa [70].

The first case of pH1N1 in Canada was reported on April 26th, and the pandemic soon followed through two waves in a bimodal fashion, with the highest hospitalization and transmission rates occurring in June and November 2009. The Government of Canada has reported over 40,000 laboratory-confirmed cases and over 400 deaths associated with pH1N1 [71]. Between April to December 2009, 4794 individuals were hospitalized due to H1N1, which was a significant increase from 1300 hospitalizations during a typical influenza season.

Excluding physician fees, the sheer number of hospitalizations resulted in over $200 million in healthcare expenditures in Canada [72]. Due to limited laboratory resources however, only hospitalized cases were tested for pH1N1, and many infected individuals with mild symptoms did not seek medical attention. Thus, the reported number of laboratory-confirmed pH1N1 cases is believed to be an underestimation of the true impact of the pandemic in Canada [71].

Since the pandemic, several studies have investigated potential risk factors associated with morbidity and mortality in pH1N1-infected patients. Kerkhove et al. undertook a meta-analysis using data from 70,000 laboratory-confirmed cases from 19 different countries**.** This study identified asthma as a major risk factor for severe cases, with asthma having been reported in 17.6% of hospitalized patients, 9.8% of Intensive Care Unit (ICU)-admitted patients, and 5.3% of pH1N1-fatal cases [73]. In hospitalized patients with asthma, pneumonia and acute respiratory distress syndrome have been identified as the most common comorbidities in pH1N1-fatal and ICU-admitted patients [74]. These studies suggest that asthmatic individuals were disproportionately affected and experienced more severe health complications during the H1N1 pandemic.

A major public health concern during the 2009 H1N1 pandemic was the considerable morbidity and mortality experienced by young asthmatic children. A study by McKenna et al. used data from 5.3 million children aged 17 or younger in the United States during the 2003-2009 influenza seasons to investigate the impact of the pandemic on the young asthmatic population. This study reported children with asthma accounted for 32% of hospitalization during a typical flu season, while they accounted for 44% of hospitalizations during the pandemic season [75]. This is while 7 million children (around 8% of the population) suffers

from asthma in the United States, thus leaving a large population of young asthmatic children at a greater risk of experiencing pandemic–associated adverse health outcomes [76].

1.5 Asthma Prevalence and Diagnosis

The WHO estimates 300 million people suffer from asthma worldwide, causing over 250,000 asthma-related deaths per year [77]. In Canada, 8.1% of the population above the age of 12 suffers from asthma, corresponding to 2.4 million Canadians [78]. Studies have identified asthma as the leading cause of hospitalizations in Canada, creating a heavy burden on the healthcare system. British Columbia spends $46 million annually on health care costs associated with asthma, excluding indirect costs such as productivity loss and time loss from work [79].

Recently, the Centers for Disease Control and prevention (CDC) reported an increase in the prevalence of asthma from 7.3% in 2001, to 8.2% in 2009 in the United States [80]. While the exact cause of this increase in asthma prevalence is not known, several studies have identified a correlation between increasing urban pollution with asthma in children [81,82]. Other studies have proposed a connection between viral infections in infancy and an elevated risk of asthma later in life [83]. However, the most well-known theory is the hygiene hypothesis, which proposes that a reduction in infectious stressors during early childhood suppresses the natural development and maturation of the immune system, resulting in a higher risk of developing allergic disease [84]. Indeed several studies have demonstrated lower rates of asthma in children living in environments with higher microbial diversity, such as farms and rural areas, than children living in urban areas [85,86]. Thus, recent urbanization trends have been suggested as the implicating factor in increased rates of asthma in the population [87].

While asthma is a complex disease with a number of different endotypes representing distinct underlying pathophysiological characteristics, allergic asthma has been reported in up to 70% of diagnosed cases [88]. Allergic asthma is characterized by a predominant Th_2 phenotype, and patients present elevated levels of IL-4, IL-5, and IL-13 (Th_2 cytokines), and airway eosinophils, mast cells, and IgE. A second endotype commonly found in adults is characterized by a predominant Th_{17} phenotype, and patients present elevated levels of sputum neutrophils and IL-17 (Th_{17} cytokine) [89]. While the Th_{17} endotype is less commonly found in the asthmatic population, IL-17 production has been implicated as the driver of more severe forms of the disease [90,91].

The diagnosis of asthma endotypes relies on the integration of a number of clinical diagnostic tools. Clinical symptoms include breathlessness, wheezing, cough, and chest tightness. Spirometry is often used as a method of quantifying lung function and airflow limitation [92]. Measuring Forced Expiratory Volume in 1 second (FEV_1) and Peak Expiratory Flow (PEF) are recommended for the diagnosis and monitoring of patients [93]. Measurements of airway hyper-responsiveness are used when there is diagnostic uncertainty following spirometry. Inhaled methacholine (or histamine) is used to measure the sensitivity of airways, and is expressed as the Provocative Concentration to cause a 20% decrease in FEV_1 (PC20). Non-asthmatics are classified as having a PC20 of 16 mg/mL or higher, while asthmatics express sensitivity at a lower concentration of methacholine depending on the severity of the disease [94]. Inflammatory markers have also been used as a method of diagnosis. Most commonly, Fractional exhaled Nitric Oxide (FeNO), which is elevated in asthma, is used to measure the degree of inflammation [95]. Serum IgE is also commonly used to determine atopic status [96].

1.6 The Inflammatory Response in Allergic Asthma

As the first line of defense to pathogens and allergens, Airway Epithelial Cells (AECs) serve as an important activator of the immune response. Upon engagement, proteases within the allergen can cleave and activate Protease Activated Receptor (PAR)-2 on AECs [97]. Activation of PAR-2 induces a pro-inflammatory response through the production of IL-6, IL-8, IL-25, IL-33, and Thymic Stromal Lymphopoietin (TSLP) [98-100]. Serine proteases within the allergen can also cleave adhesion proteins such as occludin and zonula occludens-1, thus increasing epithelial permeability and the recruitment of inflammatory mediators into the tissue [101]. Furthermore, chemokines produced by AECs, namely CCL2, CCL5, CXCL10, and CCL20, can amplify the inflammatory response by recruiting DCs [102].

Upon recruitment, DCs can be directly activated through antigen uptake. The Mannose Receptor (MR) present on DCs is involved in the recognition of the Der p 1 allergen in house-dust mites [103,104]. Interestingly, studies have identified elevated levels of MR expression on DCs obtained from asthmatic patients than healthy controls [103,105]. Furthermore, MR expression on DCs has been implicated in allergen-induced Th_2 polarization [106]. TLR-2 and TLR-4 present on DCs can also recognize allergen PAMPs including Der p 2 (an allergen present in house-dust mites), and are thus involved in the allergen-mediated activation of DCs [107,108]. DCs may also be stimulated indirectly by AEC-produced cytokines. TSLP production by AECs upregulates the expression of OX40 ligand in DCs, a molecule critical for driving the polarization of naïve $CD4^+$ T cells into Th_2 [109]. Furthermore, TSLP can induce the production of CCL22 and CCL17, critical Th_2 attracting chemokines [109]. Hence, AECs have a critical role in the DC-mediated induction of the Th_2 response in the asthmatic airway.

AEC production of IL-25 and IL-33 has also been implicated in the pathogenesis of asthma. Several studies have demonstrated an upregulation of both cytokines in asthmatic patients compared with healthy controls [110,111]. IL-33 engagement with its receptor (ST2), which is present on innate lymphoid cells 2 (ILC2), induces the production of IL-5 and IL-13 [112]. Studies have identified ILC2 production of IL-5 and IL-13 as a critical initiator of the Th_2 response [113]. Furthermore, IL-33 can directly act on in-vitro polarized $CD4^+$ Th_2 cells to stimulate the production of IL-4, IL-5 and IL-13 [114]. IL-25 also has a similar function, and can promote Th_2 differentiation in a STAT6-dependent manner [115]. Furthermore, IL-25 can act on ILC2s to induce the production of IL-13 [116].

The Th_2 cytokines IL-4, IL-5, and IL-13 have been implicated in the generation of the asthma traits. Airway eosinophilia, often described as a hallmark of asthma, is potentiated through the chemokine eotaxin [117]. Studies have demonstrated that IL-4 and IL-13 induce the production of eotaxin by airway smooth muscle cells [118]. Moreover, IL-5 can induce the differentiation of eosinophils in the bone marrow, leading to an increase in the level of eosinophils in the asthmatic airway [119]. Airway remodeling has often been described in asthma as increased mucous production, increased collagen deposition, and goblet cell metaplasia [120]. IL-4 and IL-13 can induce the expression of MUC5AC and MUC2 (genes encoding mucin proteins) in bronchial epithelial cells, thus leading to mucous hyperplasia [121]. Furthermore, IL-13 is believed to induce goblet cell metaplasia by mediating the transition of club cells to goblet cells in the airway epithelium [122,123]. IL-13 has also been demonstrated to mediate collagen deposition by fibroblasts [124].

1.7 The Th_1/Th_2 Paradigm

The Th_1/Th_2 paradigm of $CD4^+$ T cell differentiation was first introduced by Mosmann et al [125]. Since then, several studies have suggested cross-regulation of $CD4^+$ T helper cell subsets through cytokine feedback and transcriptional regulation to guide lineage fate.

Th_1 and Th_2 cell subsets are characterized based on their polarizing cytokines (cytokines that induce differentiation towards a specific subset), their effector cytokines (cytokines uniquely produced by each subset), as well as the associated transcription factors. In Th_1 cells, IL-12 and IFN-γ are defined as the polarizing cytokine, and result in the activation of the transcription factors STAT4 and T-bet. The effector cytokine associated with Th_1 cells is IFN-γ, and is involved in antiviral immunity as previously described. Conversely, IL-4 is the polarizing cytokine for Th_2 cells, and STAT6 and GATA3 are the main transcription factors driving Th_2 differentiation. The Th_2 effector cytokines include IL-4, IL-5, and IL-13, which have been implicated in the pathogenesis of asthma, as previously described [126].

A complex interplay exists during subset polarization, whereby the associated cytokines and transcription factors specific to one subset antagonize polarization towards another subset. In Th_1 cells, IFN-γ has been shown to downregulate the IL-13 response by inducing the cell-surface translocation of IL-13Rα2, the decoy receptor that binds to and suppresses IL-13 signaling [127]. Furthermore, T-bet can directly interact with GATA-3 to form a complex that can inhibit the binding of GATA-3 to its target DNA, thus repressing Th_2 lineage commitment [128]. Inversely, the expression of GATA-3 in Th_2 cells can downregulate the expression of STAT4, thus reducing the Th_1 polarizing effect of IL-12 signaling [129]. The Th_1/Th_2 paradigm is thus tightly regulated through cross-inhibition, and this method is used as a means to ensure subset adherence.

1.8 Research Aims and Rationale

Several studies have indicated excessive morbidity and mortality in asthmatic individuals during the 2009 H1N1 pandemic [73,75]. However, the immunological mechanism behind this phenomenon is unknown, and asthmatics are at a great risk of experiencing adverse outcomes in future IAV pandemics.

As previously mentioned, the Th_1-mediated immune response is involved in the induction of an antiviral state through the activation of several cell types including macrophages, DCs, and CTLs [65-67]. In contrast, allergic asthma is characterized through excessive Th_2 signaling, resulting in some of the hallmarks of asthma such as eosinophilia and lung remodeling [118-124]. Our overarching hypothesis was that asthmatics, owing to their Th_2 polarized immune response, are more susceptible to pH1N1-related morbidity, and that re-balancing of the Th_1/Th_2 immune response through pharmacologic intervention would mitigate pH1N1-mediated morbidity in asthmatics.

Aim 1: Assess the role of allergic sensitization in a murine model of pandemic influenza infection

To study the complex interplay between the Th_2 asthmatic response and the antiviral Th_1 response, we created a murine model of allergic sensitization using House Dust Mite extract (HDM). Using this model, we assessed pH1N1-mediated morbidity and characterized the immune response exhibited by sensitized mice (compared to non-sensitized mice). We hypothesized that sensitized mice would experience greater morbidity due to pH1N1 infection and express higher levels of Th_2 cytokines.

Aim 2: Assess the role of Th_2 cytokine-signaling blockade in <u>treating</u> pH1N1-related morbidity in an established infection.

To determine the role of Th_2 cytokines in pH1N1-mediated morbidity in asthmatic individuals, we blocked Th_2 signaling in our established murine model. To inhibit Th_2 cytokine signaling, we used a monoclonal antibody targeting the alpha chain of the IL-4 receptor (IL-4Rα), which conveys the signal for IL-4 and IL-13. We hypothesized that IL-4Rα blockade in sensitized mice would be an effective treatment to reduce pH1N1-mediated morbidity when an infection has already been established.

Aim 3: Assess the role of early and systematic Th_2 cytokine-signaling blockade prior to infection in <u>preventing</u> pH1N1-mediated morbidity.

To investigate the utility of IL-4Rα blockade in preventing pH1N1-related morbidity, we introduced the monoclonal antibody targeting IL-4Rα early on during sensitization, and systematically throughout the sensitization and infection experimental protocol. We hypothesized that early and systematic blockade of IL-4Rα would prevent excessive pH1N1-mediated morbidity in sensitized mice.

Chapter 2: The Role of Allergic Sensitization in the Response Towards pH1N1 Infection

2.1 Introduction

As mentioned in chapter 1, several studies have identified asthma as a major risk factor for hospitalizations associated with pH1N1 [73,75]. A mouse model of allergic asthma may provide insight on the mechanism of pH1N1-associated morbidity, and enable identification of potential therapies to protect or treat the vulnerable asthmatic population.

Although different animals have been investigated as allergic sensitization models, BALB/c mice remain the most common strain used due to their Th_2 skewing upon allergen challenge [130,131]. Different allergens as well as different routes of allergen administration have also been investigated. The protein Ovalbumin (OVA), derived from egg white, is the most commonly used method of allergic sensitization. Studies have found OVA to be effective in inducing cellular and pathophysiological phenotypes associated with human asthma. However, the antigen OVA itself is not associated with any form of human allergic sensitivity, and its clinical relevance has thus been questioned [131]. Studies have also shown that prolonged OVA exposure induces a tolerogenic response in mice, such that subsequent sensitization is associated with reduced airway eosinophils and Airway Hyper-responsiveness (AHR) [132]. Furthermore, an adjuvant (i.e. aluminum hydroxide) is required to be injected intraperitoneally alongside OVA to potentiate the development of an antigen-specific Th_2 response and other pathophysiological features [133]. Due to the systemic nature of sensitization employed by OVA, as well as the lack

of a late asthmatic response, utilization of OVA models in mice may be clinically different from human asthma.

HDM containing the allergen Der p 1 has also been investigated as a potential model of allergic asthma. HDM-sensitivity associated with elevated levels of HDM-specific IgE has been observed in 50-85% of asthmatics, making it a clinically relevant antigen [131]. Furthermore, human subjects have demonstrated both the early and the late asthmatic responses upon HDM challenge [134]. Unlike OVA, continuous exposure to HDM results in persistent eosinophilia and airway remodeling, pointing to the applicability of the HDM model in studying chronic allergic sensitization [135]. HDM-sensitized mice have also demonstrated an ability to elicit an immune response similar to that of human asthma. The proteolytic activity of HDM activates TLR-4 signaling in airway structural cells, which is essential for downstream priming of effector T helper cells [136]. Through TLR-4 signaling, HDM-sensitization can potentiate an allergic response by inducing differentiation of $CD4^+$ Th_2 cells capable of producing IL-4, IL-5, and IL-13 [137]. Airway hyper-reactivity to methacholine, eosinophilia, and airway remodeling in the form of collagen deposition and goblet cell metaplasia are characteristic of HDM sensitization in mice [135].

HDM-sensitization has been recognized as a clinically relevant model of allergic asthma, and investigators have reported using it to study virus-induced asthma exacerbations [138-141]. However, there are currently no models investigating the role of sensitization in pH1N1-related morbidity. We hypothesized that HDM-sensitization would result in greater pH1N1-mediated morbidity compared to sham-sensitized mice.

2.2 Methods

2.2.1 Animal Experimental Model

Mice

Male BALB/c mice between 6-8 weeks of age were obtained from the Jackson Laboratory (Bar Harbour, MA). Mice were housed in environmentally controlled and specific pathogen-free conditions at the Genetically Modified Models facility at the Centre for Heart Lung Innovation, St. Paul's hospital. All work was carried out in accordance with protocols approved by the University of British Columbia Animal Care and Biosafety Committees (A16-0331 and B17-0007).

Influenza Virus

While A/Puerto Rico/8/1934 remains as the most widely used H1N1 strain in murine research, studies have demonstrated distinct structural differences in the antigenic sites of its HA protein compared to that of the pandemic strain [135]. Hence, we opted to use A/California/04/2009 due to its greater relevance to the 2009 pandemic. The A/California/04/2009 strain was a kind gift from Dr. Masahiro Niikura. The initial stock was obtained from BEI Resources, and was cultivated in certified pathogen-free embryonated eggs. The Chorioallantoic Fluid (CAF) from virus-infected and non-virus infected eggs (controls) was collected using a previously described method [136]. Viral infectivity was determined using the Reef and Muench method, and is expressed as fifty percent Embryo Infectious Dose (EID_{50}) [137].

Allergic Sensitization and pH1N1 Infection

HDM from *Dermatophagoides pteronyssinus* was obtained from Greer labs (Lenoir, NC, USA). Using a previously described model of acute HDM-sensitization, mice were anesthetized

with isoflurane and intranasally exposed to either HDM (25ug of protein antigen in 35uL of sterile Phosphate-buffered Saline (PBS)) or PBS only on a daily basis [138]. Intranasal HDM/PBS exposure was performed on days -12 to -8, and -5 to -1 prior to viral infection. This was followed by a single 50uL dose of pH1N1 ($10^{6.4}$ EID_{50}/mL) on day 0 (figure 2.1). Intranasal (IN) HDM/PBS instillations then followed on days 2 to 7, and mice were sacrificed on day 8 post-viral infection (p.i.) to perform outcome measurements. Control animals received 50uL of CAF from non-virus infected eggs on day 0 instead. Animal health status and mouse weight were monitored daily throughout the 3 week experiment.

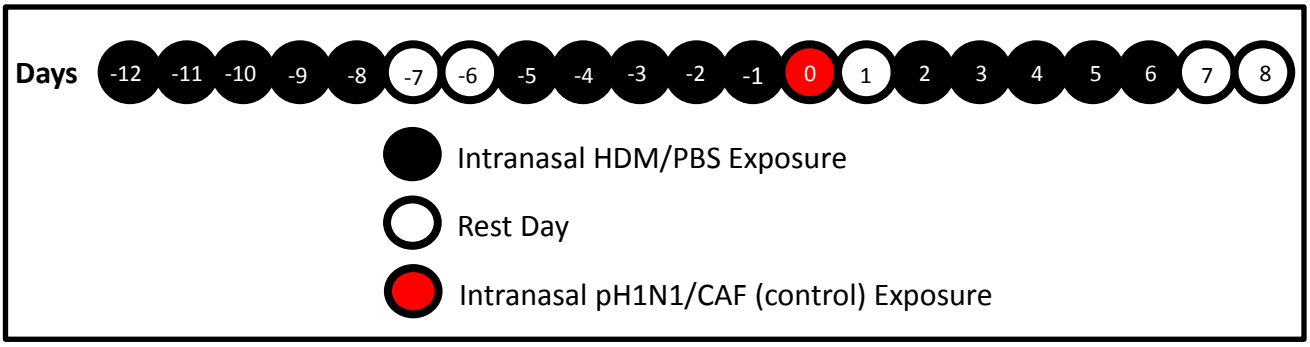

Figure 2.1 - Allergic Sensitization and pH1N1 Infection Protocol
IN HDM/PBS instillations were performed 5 days per week, for 3 consecutive weeks (marked black), and IN pH1N1 inoculation was performed on day 0 (marked red).

2.2.2 Tissue Harvest and Sample Processing

Bronchoalveolar Lavage Fluid Collection

Bronchoalveolar Lavage Fluid (BALF) was collected after euthanasia by inserting an intratracheal catheter, followed by instillation of 600uL of PBS into the bronchoalveolar space and then aspiration of the instilled fluid. The left lung lobe was clamped to ensure BALF was recovered only from the right lobe. Following recovery, the collected BALF was centrifuged at 4°C at a speed of 300xg for 10 minutes [142]. The supernatant was aliquoted and stored at -80°C

for future analysis. The pellet was re-suspended with PBS, and total cell count was performed with a hemocytometer, using a trypan blue exclusion test for cell viability.

A cyto-centrifuge (Cytospin 4 Cytocentrifuge, Thermofisher Scientific, MA, USA) was used to create slides for the re-suspended pellets. Each slide was stained with the Wright-Giemsa stain (Sigma Aldrich, MO, USA). The percentage of macrophages, eosinophils, neutrophils, and lymphocytes was calculated in a total of 200 cells, based on morphological characteristics identified under the 40x objective of a Nikon Optiphot microscope (Nikon, Tokyo Japan).

BALF Protein Detection

Concentrations of IL-13, IFN-γ, and IFN-β were measured in BALF supernatant using the MILLIPLEX MAP Mouse Cytokine/Chemokine Magnetic Bead Panel (EMD Millipore, Darmstadt, Germany) following manufacturer's protocol. The results were run on a Luminex Microplate Reader (Luminex Corporation, TX, USA).

Lung Histopathology and Morphometry

The left lung lobe was inflated with 400uL of 10% formalin, ligated at the trachea, dissected, and fixed for 24 hours in 10% formalin. Following fixation, the left lobe was cut in a transverse manner into the superior and inferior segments (figure 2.2). The inferior portion was embedded into paraffin, allowing for cross sections of the primary bronchus to be obtained. The superior portion was sectioned in a sagittal manner and embedded in paraffin, allowing for cross sections of the airways distal to the primary bronchus to be obtained [143]. Three-micron thick sections from paraffin blocks were stained with the Periodic Acid-schiff (PAS) stain to evaluate the level of goblet cell metaplasia. Slides were scanned with the Aperio ScanScope AT2, and analyzed using the Aperio ImageScope software (Leica Biosystems, Wetzlar, Germany). A colour segmentation algorithm using a predetermined signal detection threshold was applied. The

basal border of the epithelium (corresponding to the basement membrane) was traced, and the level of staining was expressed as the number of positive and strong positive pixels per um of basement membrane [144].

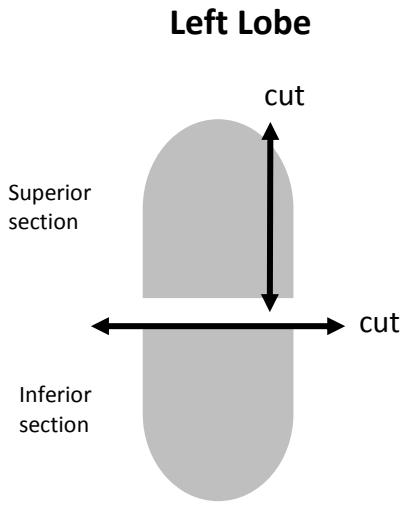

Figure 2.2 - Depiction of Left Lobe Sampling Method Following Inflation and Formalin Fixation

Lung Homogenization and RNA Extraction

Upon collection, the right lung lobe was flash frozen and stored at -80^{o}C. Lung homogenization was later performed with 500uL of PBS using a single 7mm DNAse/RNAse free stainless steel bead. Samples were shaken at 50 Hz twice at two minute intervals using the TissueLyser LT system (QIAGEN, CA, USA), and were left on ice for 30 seconds between each interval to minimize tissue degradation. RNA extraction was performing directly after homogenization using the Plus Mini Kit (QIAGEN, CA, USA) per manufacturer's protocol, and a spectrophotometer NanoDrop 8000 (Thermo Scientific, DE, USA) was used to verify RNA concentration and purity.

Viral Load Quantification

While a plaque assay is generally used to quantify viral load, we were unable to generate plaque forming units through in-vitro culture of our A/California/04/2009 strain, and hence the quantitative real-time PCR method was chosen instead.

To quantify the number of viral copies, qPCR was performed using the ROX™ qScript™ One-Step Fast qRT-PCR Kit (Quanta Biosciences, MD, USA) on RNA samples extracted from the lung homogenate. Viral RNA standards, ranging from 10^9 to 10^3 RNA copies, were extracted from avian egg amplified virus stock using a QIAamp viral RNA kit (QIAGEN, CA, USA), and viral RNA concentration and quality was measured using a Nanodrop 8000 Spectophotometer (Thermo Scientific, DE, USA). 50ng of RNA extracted from virus-fee murine lung homogenate was mixed with the standards to make the efficiency of qPCR in cellular RNA-free standards comparable to that of the samples. Samples and standards were run in triplicates on a MicroAmp® Fast Optical 96-well Reaction Plate (Thermo Fisher Scientific, ON, Canada). The primers and probe used were based on highly conserved IAV matrix gene [145], and are as follows:

5′-CTT CTA ACC GAG GTC GAA ACG-3′ (forward primer, FluA-M52C)
5′-AGG GCA TTT TGG ACA AAG/T CGT CTA-3′ (reverse primer, FluA-M253R)
Fam-CCGTCAGGCCCCCTCAAAGC-BHQ1 (probe, FluA-M96_taq)

The plate was run on a StepOne™ & StepOnePlus™ Real-Time PCR Systems (Thermo Fisher Scientific, ON, Canada), and a non-template control, which included water instead of RNA, was used in the reaction. The cycling conditions were based on manufacturer's protocol,

and are as follows: 5 minutes at 50^{o}C, 30 seconds at 95^{o}C, followed by 45 cycles of alternating setting between 3 seconds at 95^{o}C and 30 seconds at 60^{o}C. The cycle number obtained by the standards was converted into a standard curve, which was used to extrapolate the number of viral copies in the samples.

2.2.3 Statistical Analysis

Weight loss was compared using two-way Analysis Of Variance (ANOVA) followed by a Bonferroni correction. BALF total cell count and IFN-β levels were analyzed using the Mann-Whitney test due to the presence of outliers. All other data, including goblet cell staining, viral titre, and the cytokine multiplex data (IL-4, IL-5, and IFN-γ) were analyzed using a two-tailed Student's t-test. Data are expressed as mean ± SEM, and p-values < 0.05 were considered significant. All statistical analysis was performed using GraphPad Prism version 5 (La Jolla, CA).

2.3 Results

2.3.1 BALF Inflammatory Profile Following Acute HDM Exposure

We sought to determine the efficacy of HDM sensitization in producing an asthma-like phenotype in mice. Mice were intranasally exposed to HDM or PBS for 3 weeks, 5 times per week. Upon sacrifice, BALF was collected from the right lobe, and cytospin was performed on the cell pellet. The Wright-Giemsa-stained BALF slides were counted under a microscope, and cell types were identified based on morphological characteristics. To account for differences in the total cell count observed between samples (figure 2.3A), cell differentials are expressed as a percentage of 200 counted cells. HDM-sensitized mice present significantly reduced percentage

of BALF macrophages (figure 2.3B). This was accompanied by an increase in the percentage of BALF eosinophils, neutrophils, and lymphocytes (figure 2.3C-E).

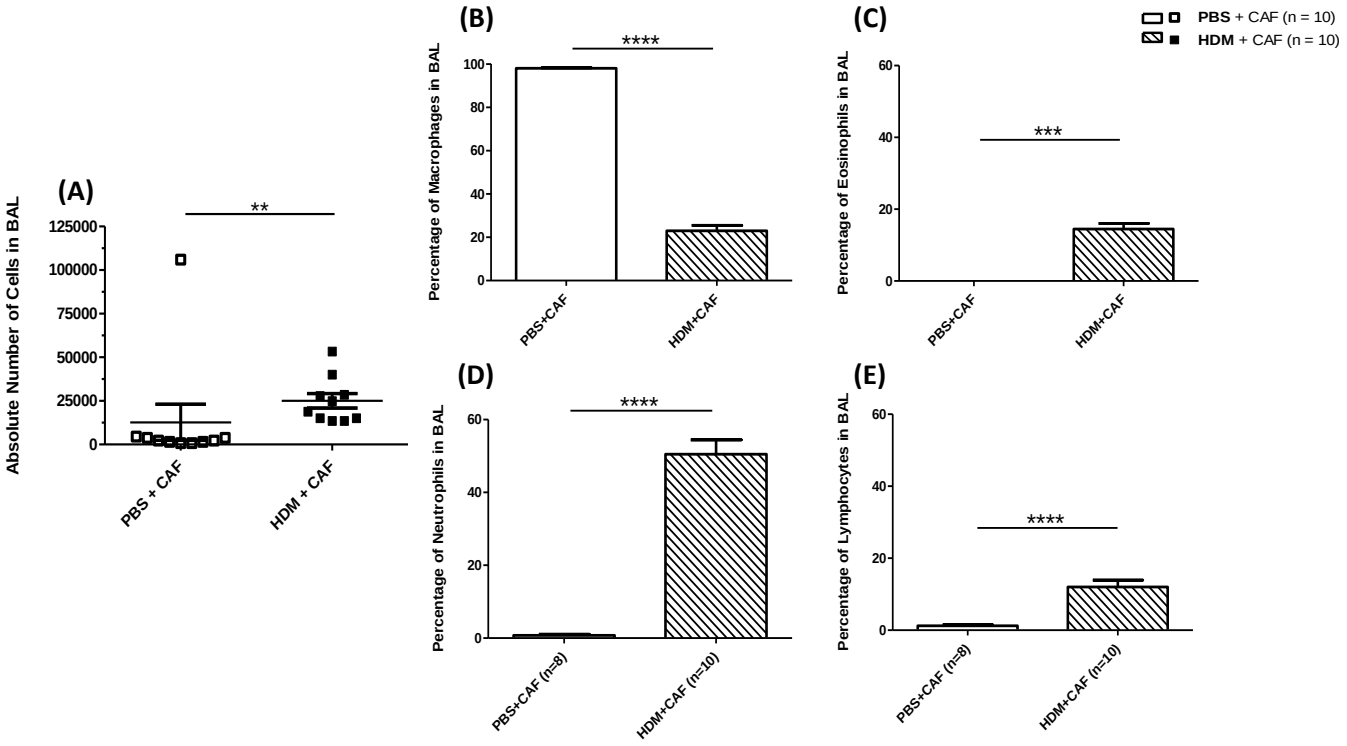

Figure 2.3 - BALF Macrophage and Eosinophil Cell Differentials Following HDM-sensitization

BALF was collected on day 8 p.i. from the right lobe. (A) Cells were counted under the microscope using a hemocytometer with the trypan blue exclusion test to determine the total number of cells in the samples. A cytospin was made from the pellet, and the percentage of (B) Macrophages, (C) Eosinophils, (D) Neutrophils, and (E) Lymphocytes between HDM-sensitized and PBS-exposed mice in a total of 200 counted cells is shown. Data are expressed as mean ± SEM. *** $p<0.001$, **** $p<0001$ by (A) Mann-Whitney test and (B-E) Student's t-test.

2.3.2 Airway Remodeling Following Acute HDM Exposure

To determine the extent of airway remodeling caused by HDM exposure, paraffin embedded lung sections were stained with PAS to visualize goblet cells. A colour segmentation algorithm with a pre-determined signal detection threshold was used to quantify the level of staining. To account for differences in the size of analyzed airways, results were normalized to the length of the basal membrane, and data are represented as the number of positively-stained

pixels per um of basement membrane. HDM-sensitized mice displayed extensive PAS staining representative of goblet cell metaplasia (figure 2.4) compared to PBS-exposed mice, pointing to the potential role of HDM in airway remodeling.

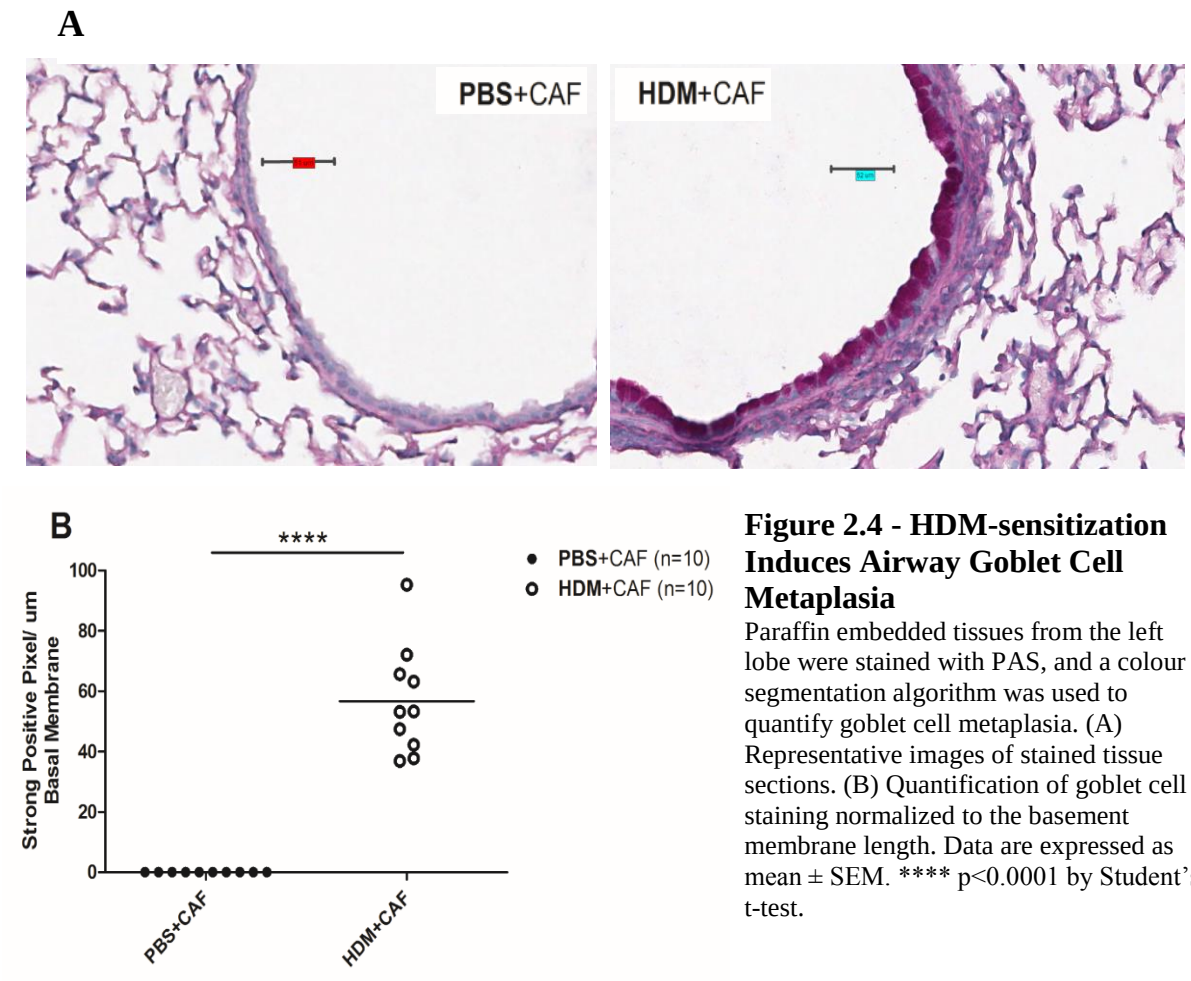

Figure 2.4 - HDM-sensitization Induces Airway Goblet Cell Metaplasia
Paraffin embedded tissues from the left lobe were stained with PAS, and a colour segmentation algorithm was used to quantify goblet cell metaplasia. (A) Representative images of stained tissue sections. (B) Quantification of goblet cell staining normalized to the basement membrane length. Data are expressed as mean ± SEM. **** $p<0.0001$ by Student's t-test.

2.3.3 HDM-sensitized Mice Experience Greater Morbidity Following pH1N1 Infection

In order to determine the relationship between sensitization and morbidity, CAF-exposed mice that were HDM-sensitized or PBS-exposed were weighed daily. Compared with PBS-exposed mice, HDM sensitization alone did not result in weight loss before or after CAF treatment (figure 2.5). To determine the role of sensitization on influenza exacerbation, we

monitored pH1N1-infected mice for weight loss as an indicator of disease severity. In contrast to CAF-treatment, HDM-sensitized mice experienced greater weight-loss on days 7-8 following pH1N1 infection (figure 2.6A). To explore whether the observed increase in weight-loss was related to viral clearance, qPCR was performed on the homogenized lungs of mice on day 8 p.i. HDM-sensitized mice demonstrated significantly higher levels of viral copies compared with PBS-exposed mice (figure 2.6B).

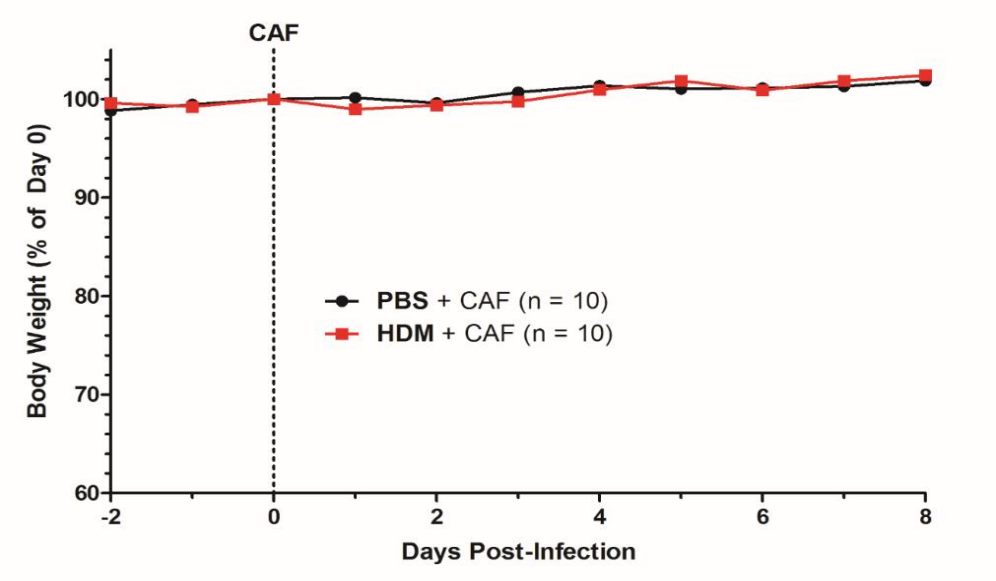

Figure 2.5 - Body Weight Changes Following HDM-sensitization
Mice were exposed intranasally to HDM or PBS for 3 weeks. A single IN inoculation of CAF was performed on day 0. Mice were weighed daily, and mean change in body mass is plotted. Weight is expressed as a percentage of weight on day 0. Data represent two independent experiments, and are compared using two-way ANOVA with a Bonferroni correction.

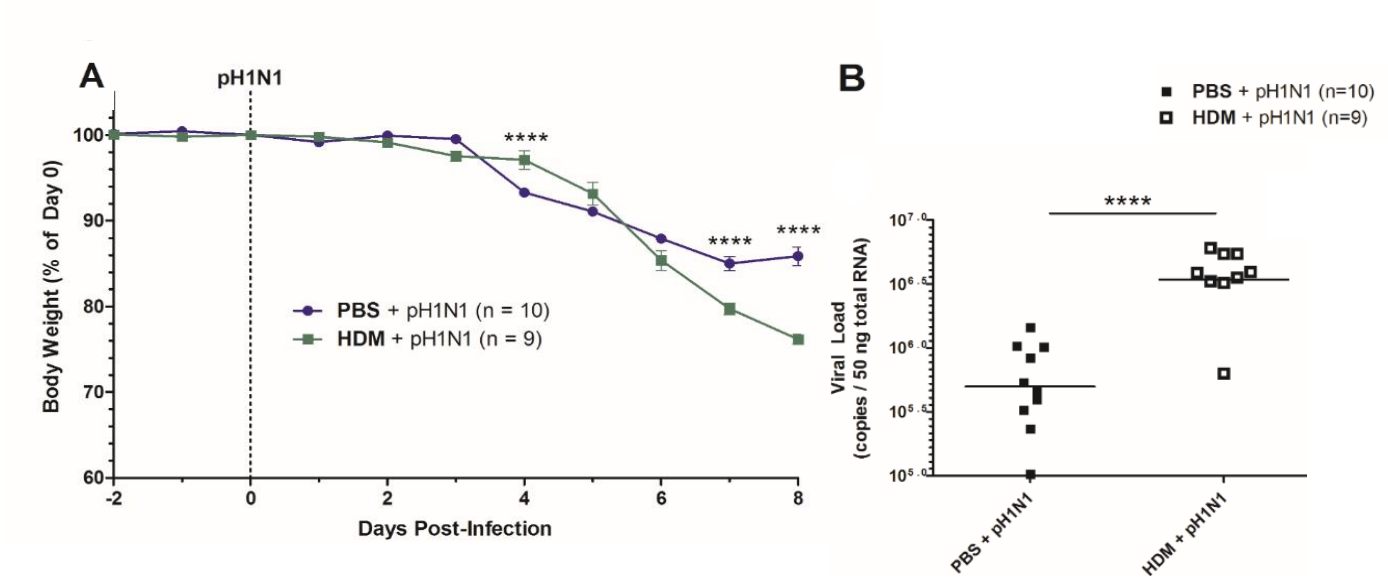

Figure 2.6 - HDM-sensitization Induces Greater Weight Loss and Elevated Viral Loads Following pH1N1 Infection

Mice were exposed intranasally to HDM or PBS for 3 weeks, and intransally infected with $10^{6.4}$ EID_{50}/mL of pH1N1 on day 0. (A) Mice were weighed daily, and the mean change in body mass is plotted as a percentage of weight on day 0. (B) Viral load is quantified using qPCR, and is expressed as the number of copies per 50ng of total RNA. Data represent two independent experiments. **** $p<0.0001$ by (A) two-way ANOVA with a Bonferroni correction and (B) Student's t-test.

2.3.4 BALF Cytokine Profile Changes Induced by HDM-sensitization

Next, we aimed to determine whether HDM-sensitized mice express an altered immune response. Using a multiplex assay, we measured IFN-γ, IFN-β, and IL-13 in the BALF supernatant of HDM-sensitized and PBS-exposed mice infected with pH1N1. IFN-γ protein levels (Th_1 marker) are significantly reduced in HDM-sensitized mice (figure 2.7A). In contrast, BALF IL-13 levels (Th_2 marker) are significantly upregulated upon HDM-sensitization (figure 2.7B). IFN-β was measured as a marker of the innate immune response. Our findings indicated significantly elevated levels of IFN-β in HDM-sensitized mice.

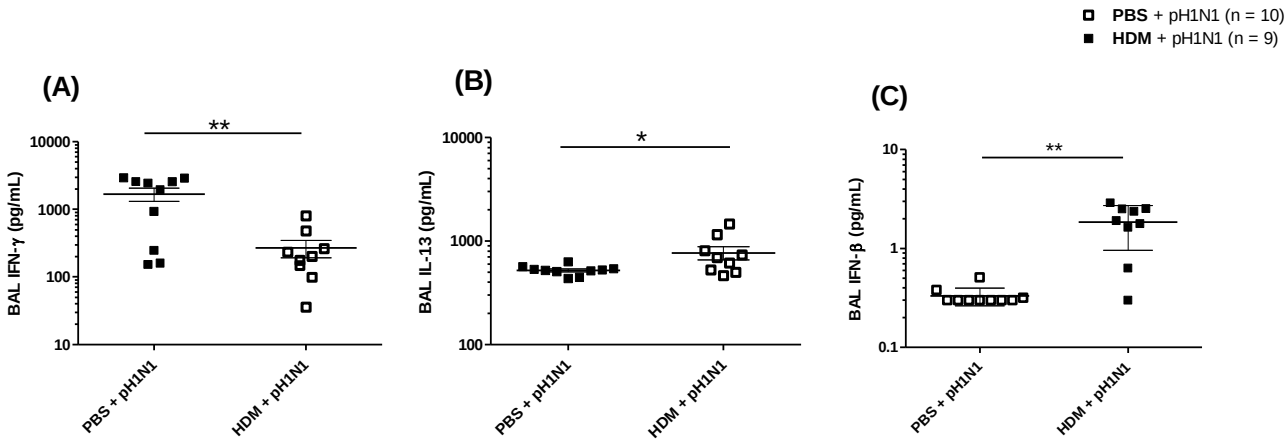

Figure 2.7 - HDM-sensitization Alters BALF Cytokine Levels in pH1N1-infected Mice
BALF was collected from the right lobe. (A) IFN-γ, (B) IL-13, and (C) IFN-β levels were quantified using a multiplex assay. Data are expressed as mean ± SEM. *p<0.05, **p<0.01 by (A-B) Student's t-test and (C) the Mann-Whitney Test.

2.4 Discussion

Although HDM models have been previously utilized to investigate asthma exacerbations, the application of HDM-sensitization in pH1N1-mediated morbidity has yet to be investigated. We hypothesized that HDM-sensitized mice would experience greater pH1N1-mediated morbidity compared to CAF-exposed mice.

Using a previously validated model of HDM-sensitization, we have been able to create an allergic airway phenotype which is likely relevant to human asthma [146]. Our results in CAF-exposed mice indicate that HDM-sensitization leads to an influx of eosinophils, as demonstrated by a 14.5-fold increase in the percentage of BALF eosinophils, which is consistent with other 4-week and 8-week models of HDM-sensitization [147]. This increase in BALF eosinophils was associated with a 4.3-fold decrease in the percentage of BALF macrophages. This reduction in the percentage of BALF macrophages may be attributed to a large influx of eosinophils into the

airways. HDM-sensitization also led to increased levels of PAS staining indicative of goblet cell metaplasia, one of the hallmark characteristics of allergic asthma [147].

To investigate the role of allergic sensitization in pH1N1-mediated morbidity, we recorded weight prior to and after pH1N1 infection in HDM-sensitized and PBS-exposed mice. To account for genetic and dietary differences, weight was expressed as a percentage of day 0 (day of pH1N1 infection). Mice experienced significantly greater weight-loss and reached their humane endpoint by day 8 p.i. Although all mice experienced similar levels of weight-loss at the beginning of the infection, PBS-exposed mice stabilized their weight by day 7-8 p.i. However, HDM-sensitized mice continued to lose weight. Interestingly, HDM-sensitization alone did not cause weight-loss in mice, and only exacerbated pH1N1-mediated weight loss.

To investigate a potential mechanism involved in excessive pH1N1-mediated weight loss, we measured the number of viral copies using qPCR. Interestingly, HDM-sensitized mice displayed a 6.9-fold increase in the number of viral copies on day 8 p.i., pointing to increased viral burden as a potential explanation for excessive weight-loss. Although eosinophils have been shown to contribute to antiviral immune response [148], elevated pulmonary eosinophils in this model were not associated with reduced viral burden.

To assess the airway microenvironment, we measured cytokines in BALF using a multiplex assay. IL-13 has been described as a bio-signature of asthma due to its involvement in the recruitment of eosinophils to the airways, and has been used as a marker of Th_2 polarization [137,149]. Consistent with previous literature, we found elevated BALF levels of IL-13 in HDM-sensitized mice, as compared with PBS-exposed mice. Furthermore, we measured IFN-β as a marker of innate immunity. While there is a lack of studies that have measured IFN-β production in the asthmatic airway following IAV challenge, other studies have reported dampened

production of IFN-β in bronchial epithelial cells of asthmatic patients following RV infection [150]. This is in contrast to our findings, which indicate that sensitized mice present elevated IFN-β in BALF following pH1N1 infection. Although differences in our findings may be due to the use of a different virus, it may also be attributed to variation in methodology; Wark et al. measured IFN-β production 48 hours following viral infection, whereas we measured IFN-β in BALF 8 days after pH1N1 infection [150]. Hence, our findings may point towards sustained IFN-β production in a longer term infection model.

Although IFN-γ is characterized as a marker of Th_1 polarization and is an important antiviral cytokine, its exact role in the pathogenesis of asthma is controversial. Studies have reported elevated levels of IFN-γ mRNA in BALF cells from severe asthma patients [151]. Furthermore, stimulation of macrophages by IFN-γ has led to steroid resistance and AHR in mice [152]. Other studies however, have reported an inhibitory function for IFN-γ in mucous hypersecretion and eosinophilia [153]. In our model of allergic sensitization, we found reduced levels of IFN-γ, pointing to a potential mechanism whereby the antiviral defense may be dampened.

Taken together, our results indicate that HDM-sensitization may increase susceptibility to pH1N1-mediated morbidity due to elevated levels of viral load. This is associated with elevated BALF IL-13 and IFN- β, and dampened BALF IFN-γ protein levels. This model of allergic sensitization can be used to investigate potential treatments for pH1N1 infection.

Chapter 3: IL-4Rα Blockade as a Treatment in Established pH1N1 Infection in a Mouse Model of Allergic Asthma

3.1 Introduction

3.1.1 Th_1/Th_2 Imbalance in Asthma Exacerbations

Several studies have identified viral infections as a major cause of asthmatic exacerbation, with asthmatics experiencing higher viral loads, greater lower respiratory symptoms, increase in bronchial hyper-reactivity, as well as lung function impairment in response to Rhinovirus (RV) infection [154]. Insults to the immune system causing alterations in the Th_1/Th_2 balance have been suggested as an inducer of asthmatic exacerbation [155].

As the first barrier to pathogens, AECs have been identified as major producers of IL-25 and IL-33 [115,156]. Upon release, both cytokines induce Th_2 cells and ILC2s to produce IL-5 and IL-13, skewing the immune response towards Th_2 polarization [114,115,157]. Asthmatics present elevated baseline IL-25 expression, which is augmented upon RV infection in a mouse model of asthma [111]. IL-33 has also been implicated in RV-induced exacerbations, with elevated IL-33 correlating with higher viral load and elevated BALF IL-5 and IL-13 [158]. Furthermore, RV-induced exacerbations have been associated with a deficient IFN-γ and IL-10 response, and an augmented IL-4, IL-5, and IL-13 response, corresponding to skewing towards a Th_2 phenotype [154].

3.1.2 Current Treatments for Asthma: Restoring the Th_1/Th_2 Balance

Due to the role of the Th_2 response in asthma and asthma exacerbations, blocking this response has been of clinical interest for many years. A phase II clinical trial of Altrakincept, a soluble IL-4 receptor that binds to and quenches IL-4 signaling, demonstrated improvements in FEV_1, stabilization in asthma symptom scores, and significantly lower requirement for β2-agonist use [159]. Despite its effectiveness in reducing asthma symptoms, Altrakincept treatment showed no significant difference in the exacerbation rate of patients [160]. Treatment with Lebrikizumab, a monoclonal antibody targeting IL-13, showed 5.5% mean increase from baseline FEV_1 in patients with uncontrolled asthma [161]. Furthermore, Lebrikizumab treatment in mild-asthmatic patients showed reduced serum IgE and a non-significant reduction in the late phase response following allergen challenge [162]. However, Lebrikizumab treatment did not significantly reduce exacerbation rates in asthma [161]. Mepolizumab, a monoclonal antibody against IL-5 which is now approved for treatment of eosinophilic asthma, has shown promise in controlling severe asthma [163]. Ortega et al. demonstrated up to 100 mL mean increase from baseline FEV_1, and 0.42 points improvement in the asthma control questionnaire in patients receiving Mepolizumab [164]. Mepolizumab was also able to reduce asthma exacerbation rates by 53%, pointing to the applicability of this treatment in the healthcare setting [164]. However, there is no information regarding the efficacy of this antibody specifically against virus-induced asthma exacerbations.

Dupilumab, a monoclonal antibody targeting IL-4Rα (also known as CD124), which has been recently approved by FDA for treatment of severe asthma, significantly reduces exacerbation rates [165,166]. In glucocorticoid-dependent severe asthma, Dupilumab was able to cause a 70.1% reduction in glucocorticoid dose, as well as a 220 mL increase from baseline

FEV_1 [167]. Another study by Wenzel et al. showed an 87% reduction in asthma exacerbation in moderate to severe asthmatic patients receiving Dupilumab. Furthermore, patients in this study had reduced serum biomarker levels of Th_2 inflammation, namely IgE, eotaxin-3, and CCL17 [168]. In mice, blocking IL-4Rα signaling has showed significant reduction in HDM-induced AHR, lung eosinophilia, and goblet cell metaplasia [169].

3.1.3 Interleukin-4 Receptor Alpha Signaling

IL-4Rα chain is shared for signaling by two of the driving cytokines behind the Th_2 response, namely IL-4 and IL-13. For IL-13 to induce signaling, it binds with low affinity to IL-13Rα1, which requires recruitment and hetero-dimerization with IL-4Rα for a high affinity interaction [170]. IL-13 can also bind to IL-13Rα2, which is a high-affinity decoy receptor used to quench IL-13 signaling [171]. In contrast, IL-4 binds with high affinity to IL-4Rα when it is hetero-dimerized with one of two receptor chains, either the IL-13Rα1 or the γC chain [172].

IL-4/IL-13 signaling, and the subsequent dimerization of the IL-4Rα with the respective complex chain results in the activation of Janus kinases (JAK). Each receptor subunit is associated with a specific JAK in its cytoplasmic domain; IL-4Rα is associated with JAK1, γC is associated with JAK3, and IL-13Rα1 is associated with either JAK2 or Tyrosine Kinase (TYK)-2 [173]. JAK activation results in the phosphorylation of tyrosine residues in the cytoplasmic domain of IL-4Rα, which acts as a docking site for molecules containing Src homology 2 (SH2) domains, such as STAT6 [173]. Upon recruitment, STAT6 is tyrosine phosphorylated, disengages from the receptor domain, homo-dimerizes, and migrates to the nucleus [174]. Within the nucleus, STAT6 binds to consensus sequences within promoters of IL-4 and IL-13 regulated genes, resulting in their upregulation. An alternative mechanism has also been proposed,

whereby IL-4 (and not IL-13) signaling results in the recruitment of Insulin Receptor Substrate (IRS)-2, leading to the activation of the Phosphoinositide-3-Kinase (PI3K) pathway [175]. Activation of the PI3K pathway is thought to promote Th_2 cell survival by downregulating the apoptosis of lymphocytes [176].

IL-4/IL-13 signaling and STAT6 activation have been linked to several hallmarks of asthma, including increased mRNA expression of MUC5AC and MUC2 in primary bronchial epithelial cells (resulting in increasing mucous production) [121], increased production of eotaxin (an eosinophil chemoattractant) by airway smooth muscle cells [118], as well as enhancement of G Protein-coupled Receptor (GPCR)-associated calcium signaling (resulting in airway smooth muscle contractility) [177]. In contrast, IL-4Rα expression is downregulated following acute viral infection in $CD8^+$ T cells, and an elevated IL-4Rα expression correlates with poor antiviral immunity due to lower production of antiviral TNF-α and IFN-γ [178]. Hence, the question arises as to whether enhanced IL-4/IL-13 signaling through IL-4Rα following allergen challenge results in viral exacerbations and poor health outcomes. We hypothesized that blocking IL-4Rα would reduce pH1N1-mediated morbidity in HDM-sensitized mice.

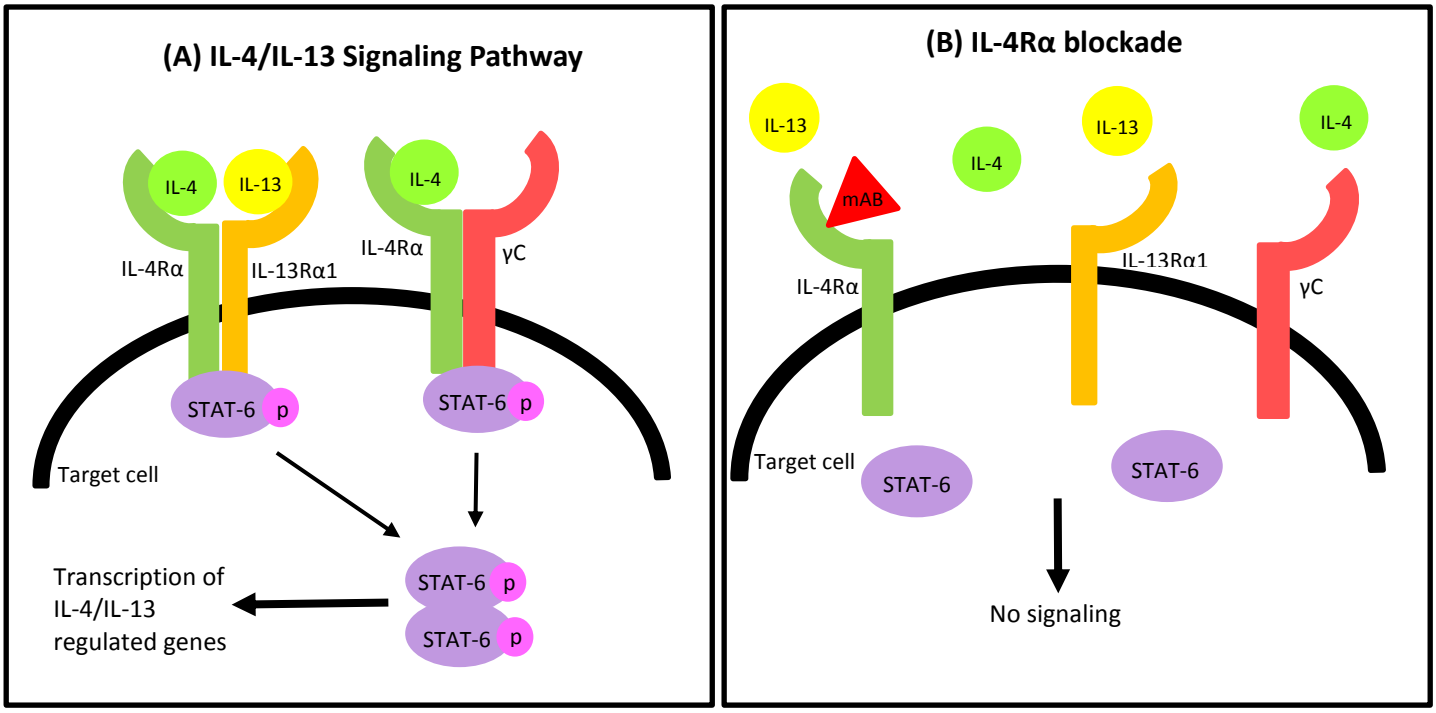

Figure 3.1 - IL-4Rα Signaling Pathway and Blockade
(A) IL-4/IL-13 Signaling Pathway. IL-4 binds directly to IL-4Rα, and recruits either IL-13Rα1 or γC for hetero-dimerization. Conversely, IL-13 binds to IL-13Rα1 to induce its hetero-dimerization with IL-4Rα. Upon hetero-dimerization, the signal transduction cascade induces the phosphorylation of STAT-6, which homo-dimerizes and acts as a transcription factor to upregulate the expression of IL-4 and IL-13 regulated genes. (B) IL-4Rα blockade. Using a monoclonal Antibody (mAB) targeting IL-4Rα prevents IL-4 and IL-13 signaling, thus inhibiting downstream STAT6 phosphorylation and transcriptional activity.

3.2 Methods

Animal Experimental Protocol

As described in chapter 2, male BALB/c mice between 6-8 weeks (Jackson Laboratories, Bar Harbour, MA) were intranasally sensitized with HDM (*Dermatophagoides pteronyssinus,* 25ug of protein in 35uL of sterile PBS), or PBS only on a daily basis [138]. IN HDM/PBS exposure was performed on days -12 to -8, and -5 to -1 prior to and on days 2 to 7 following viral infection. A single 50uL dose of pH1N1 ($10^{6.4}$ EID_{50}/mL) was intranasally instilled on day 0 (figure 3.1).

Anti-IL-4Rα (4-3, hybrid IgG1) and IgG1 control (4G8) monoclonal antibodies were obtained from Amgen (Seattle, WA), and 2mg of each antibody diluted in PBS was administered intraperitoneally (IP) per respective animal group, as previously described [173]. The volume of PBS used for the delivery of the antibodies was based on 10uL of PBS per gram of mouse weight. IP injections were performed on days 1 and 6 following pH1N1 infection, to create a treatment model in an established viral infection. Control mice received IP injections of PBS on corresponding days, and were intranasally instilled with either PBS or HDM. Animal health status and weight were monitored daily, and mice were sacrificed on day 8 p.i. to perform outcome measurements.

Four groups of animals were studied: (1) PBS-control (IN PBS / IP PBS), (2) HDM-control (IN HDM / IP PBS), (3) anti-IL-4Rα treatment (IN HDM / IP anti-IL-4Rα), and (4) IgG isotype control (IN HDM / IP IgG).

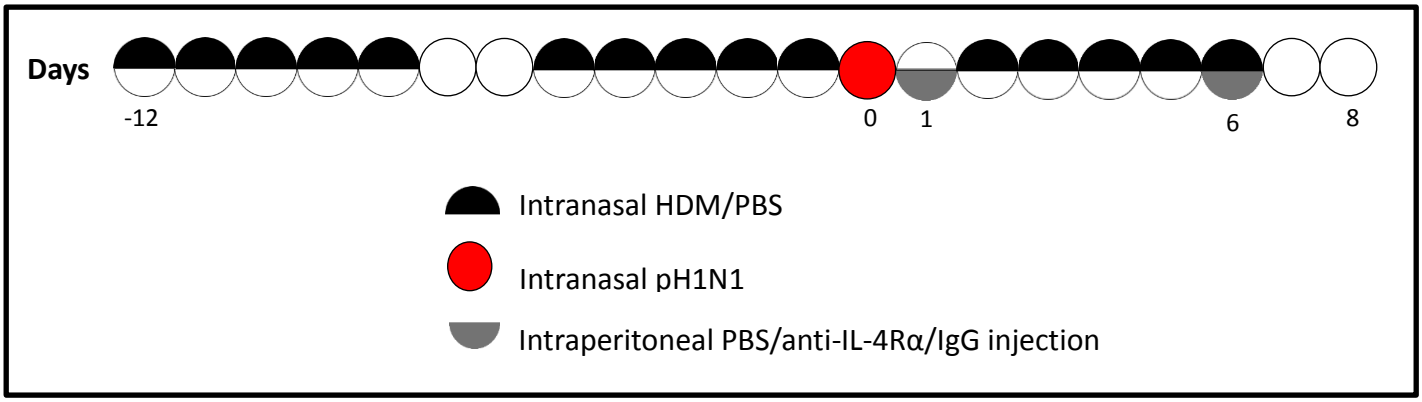

Figure 3.2 – Anti-IL-4Rα Treatment Experimental Protocol
IN HDM/PBS instillations were performed 5 days per week, for 3 consecutive weeks (marked black). IN pH1N1 inoculation was performed on day 0 (marked red), and IP PBS/anti-IL-4Rα/IgG injections were performed on days 1 and 6 following pH1N1 infection (marked gray).

Ethics Statement

All work was carried out in accordance with protocols approved by the University of British Columbia Animal Care and Biosafety Committees (A16-0331 and B17-0007).

Tissue Harvest and Sample processing

BALF collection, Right lobe homogenization and RNA extraction, left lobe histology and morphometry measurements, as well as viral load quantification were performed as previously described in chapter 2.

BALF Protein Detection

Concentrations of IL-4, IL-5, IL-17A, and IFN-γ were measured in BALF supernatant using the MILLIPLEX MAP Mouse High Sensitivity T cell Panel (EMD Millipore, Darmstadt, Germany) following manufacturer's protocol. The results were run on the Luminex Microplate Reader (Luminex Corporation, TX, USA). The Verikine-HS Mouse Interferon Beta Serum ELISA Kit (PBL Assay Science, NJ, USA) was used to measure IFN-β in BALF supernatant, and a Versamax Microplate Reader (Molecular Devices, San Jose, CA) was used to measure optical density in the samples.

An in-house ELISA was used to measure IgG antibodies made against pH1N1 epitopes. 96 well ELISA plates were incubated overnight at 4^{o}C with pH1N1 viral stock inactivated with Triton X-100. BALF samples were added the next day and incubated at room temperature for 1 hour. A monoclonal antibody against recombinant H3 HA from Influenza - A/Brisbane/10/2007 (H3N2) (clone: AT179.705.161 - Influenza Reagent Resource, VA, USA) was used as a negative control.

Peroxidase AffiniPure Donkey anti-mouse IgG (Jackson ImmunoResearch Laboratories, PA, USA) was used as the secondary antibody, and was incubated for 45 minutes at room temperature. The samples were developed after a 5 minute incubation with 3-ethylbenzothiazoline-6-sulphonic acid, and the optical density was measured using a Victor X5 – 2030 multilabel plate reader (Perkin Elmer, Waltham, MA) at 405 nm. BALF previously

collected from virus-infected mice (n=4) and non-infected mice (n=3) served as positive and negative controls respectively.

Statistical analysis

Weight-loss was compared using a two-way ANOVA with Bonferroni correction for multiple testing. All other parameters were tested for normality using the D'Agostino and Pearson omnibus normality test. Parameters that were normally distributed ($p \geq 0.05$), namely BALF eosinophil, macrophage, and neutrophil differentials, BALF IL-4 levels, goblet cell metaplasia, and viral titres, were analyzed using a two-tailed Student's t-test. Parameters that were not normally distributed ($p < 0.05$), namely BALF total cell count and lymphocyte differentials, as well as BALF IFN-β, IFN-γ, IL-5, and IL-17A levels were analyzed using a Mann-Whitney U test. Data are expressed as mean ± SEM, and p-values < 0.05 were considered significant. All statistical analysis was performed using GraphPad Prism version 5 (La Jolla, CA).

3.3 Results

3.3.1 Anti-IL-4Rα Treatment Reduces Excessive pH1N1-mediated Morbidity in HDM-sensitized Mice

To examine the role of IL-4Rα blockade treatment in pH1N1-mediated morbidity, mice were weighed over the course of the experiment. Similar to our findings in chapter 2, HDM-control mice (IN HDM / IP PBS) lost significantly more weight than PBS-control mice (IN PBS / IP PBS) (figure 3.3A). Comparing treatment groups, HDM-sensitized mice treated with anti-IL-4Rα (IN HDM / IP anti-IL-4Rα) experienced significantly lower weight loss than their IgG-

exposed counterparts (IN HDM / IP IgG) (figure 3.3B). In order to examine the role of IL-4Rα blockade treatment on viral burden, qPCR was performed on the lung homogenate to determine the number of pH1N1 viral copies. HDM-control mice presented significantly higher viral loads than PBS-control mice (figure 3.3C), consistent with our findings from chapter 2. Furthermore, the anti-IL-4Rα treatment group presented significantly lower number of viral copies than the IgG isotype control group (figure 3.3D).

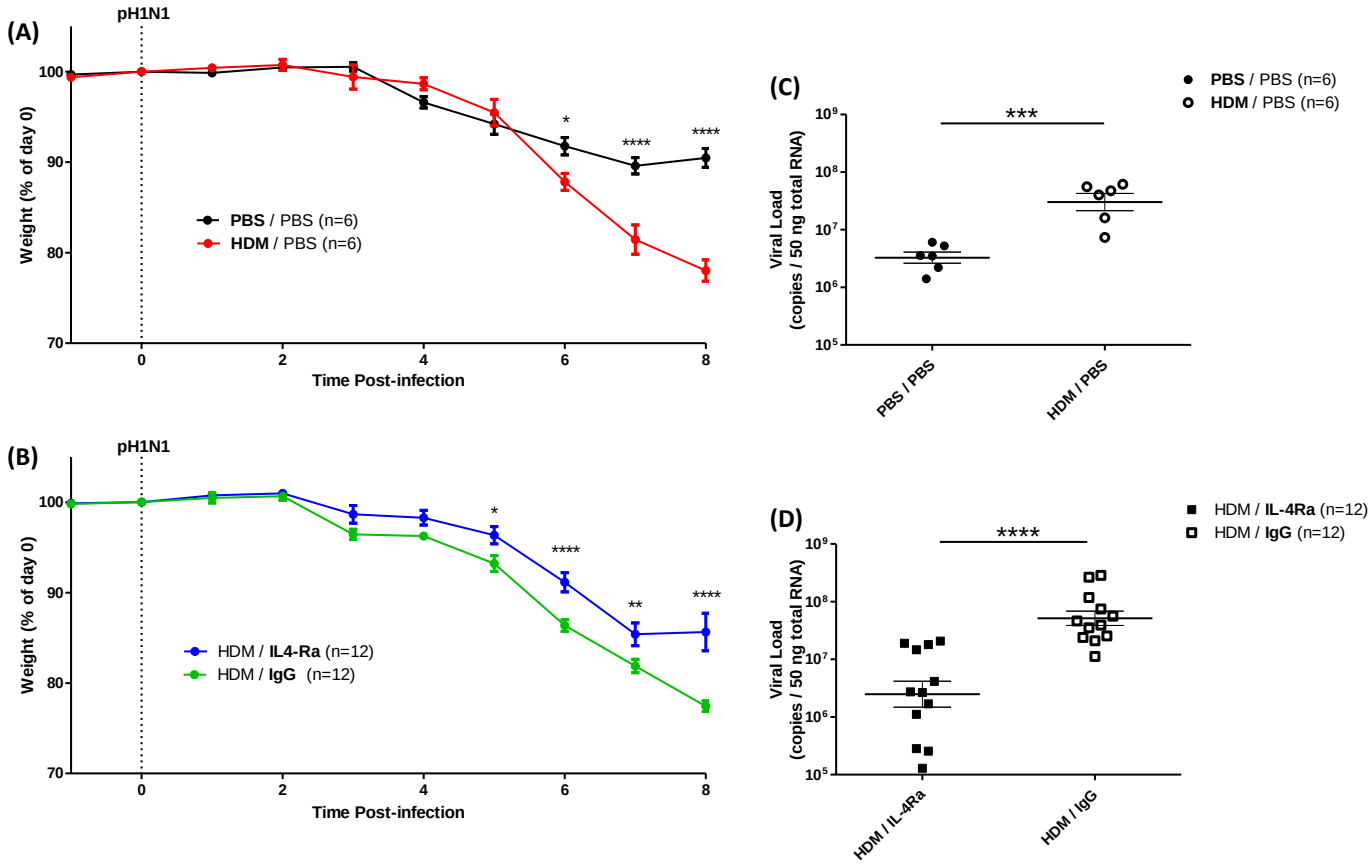

Figure 3.3 – Anti-IL-4Rα Reduces pH1N1-mediated Weight Loss and Excessive Viral Load in HDM-sensitized Mice

Mice were intranasally exposed to HDM or PBS for 3 weeks, and IP injected 1 and 6 days after pH1N1 infection with either PBS only, anti-IL-4Rα, or IgG isotype control. (A-B) Mice were weighed daily, and the mean change in body mass is plotted as a percentage of weight on day 0. (C-D) Viral load was quantified using qPCR on the homogenized right lobe, and is expressed as the number of copies per 50ng of total RNA. Data represent two independent experiments, and are expressed as mean ± SEM. * $p<0.05$, ** $p<0.01$, **** $p<0.0001$ by (A) two-way ANOVA with a Bonferroni correction and (B) Student's t test.

While anti-IL-4Rα treatment significantly reduced HDM-mediated excessive weight loss, these mice still experienced greater weight loss than PBS-control mice (figure 3.4A). However, no significant difference was found in the number of viral copies between the anti-IL-4Rα treatment and PBS-control groups (figure 3.4B)

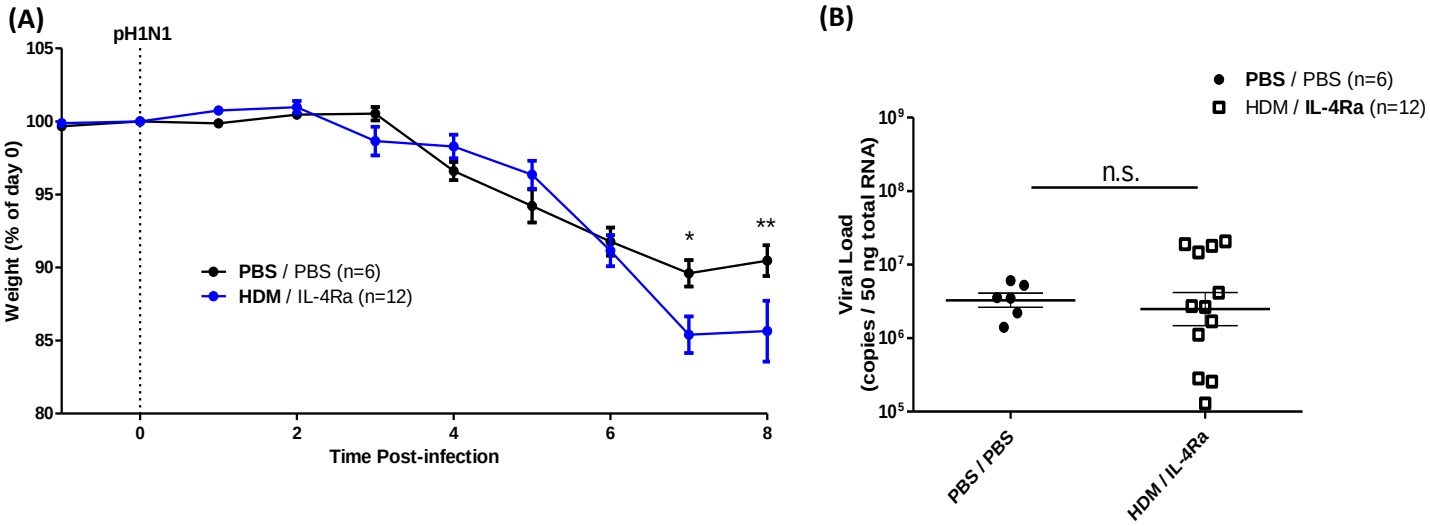

Figure 3.4 – Anti-IL-4Rα treatment Group Experienced Greater Weight Loss but Similar Viral Loads Compared to PBS-control Group Following pH1N1 Infection
(A) Mice were weighed daily, and the mean change in body mass is plotted as a percentage of weight on day 0. (B) Viral load was quantified using qPCR on the homogenized right lobe, and is expressed as the number of copies per 50ng of total RNA. Data represent two independent experiments, and are expressed as mean ± SEM. * $p<0.05$, ** $p<0.01$, by (A) two-way ANOVA with a Bonferroni correction and (B) Student's t test.

3.3.2 Anti-IL-4Rα Treatment is Insufficient in Restoring the BALF Immune Cell Composition

We sought to determine whether IL-4Rα blockade treatment restored BALF immune cell composition. Similar to our previous findings, we found no significant difference in the concentration of immune cells between the PBS-control and HDM-control groups (figure 3.5A) or between the anti-IL-4Rα treatment and the IgG isotype control groups (figure 3.6A). A BALF cytospin was then created to determine immune cell composition between samples. HDM-

control mice had increased percentage of eosinophils and reduced percentage of macrophages compared to PBS-control mice (figure 3.5B and C), in agreement with our findings from chapter 2.

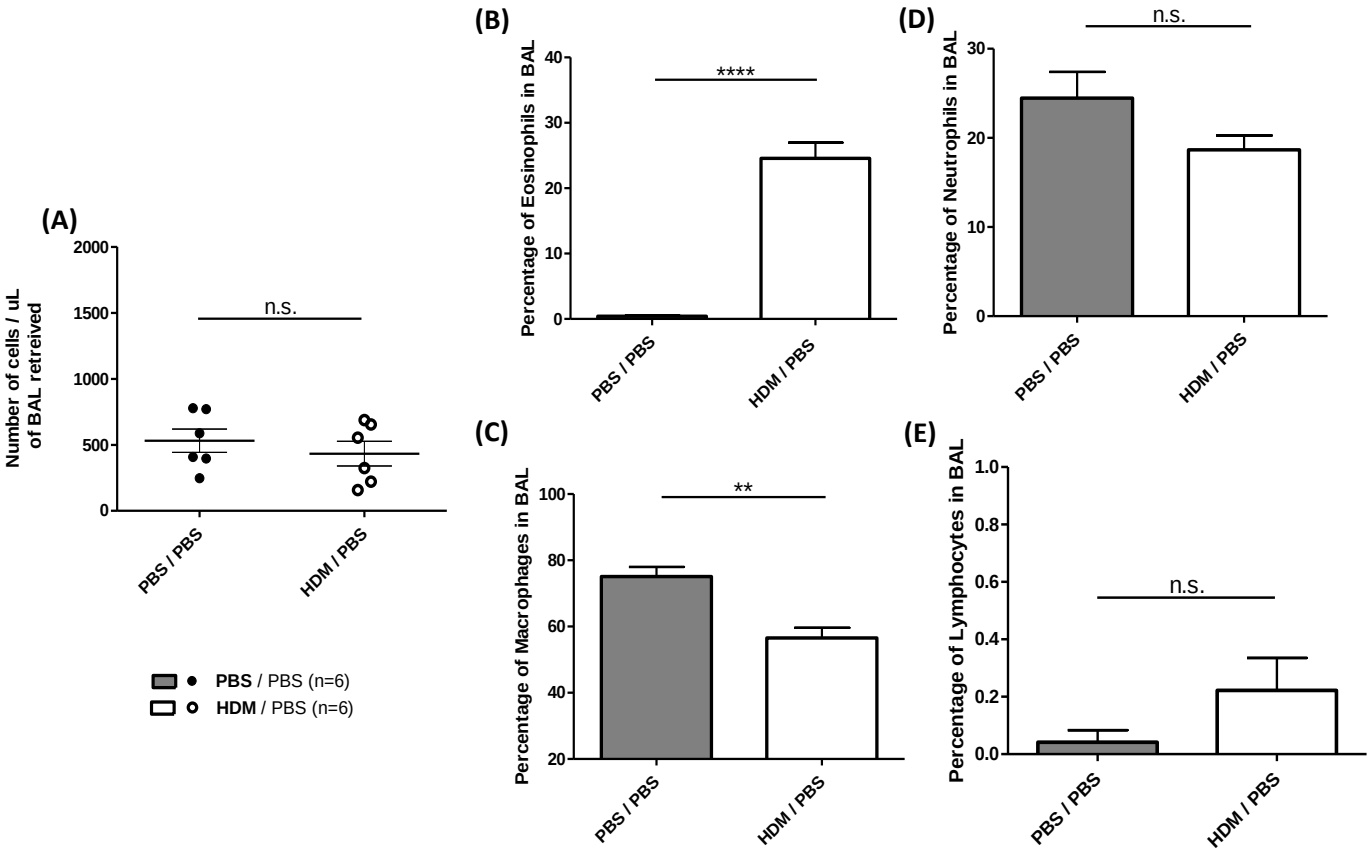

Figure 3.5 - BALF Cell Differentials in PBS-control and HDM-control Groups
BALF was collected on day 8 p.i. from PBS-exposed and HDM-sensitized mice. (A) Cells were counted using a hemocytometer, and are expressed as the number of cells per micrlotre of BALF retrieved. A cytospin was made from the cell pellet, and the percentage of (B) Eosinophils, (C) Macrophages, (D) Neutrophils, and (E) Lymphocytes was determined in a total of 200 counted cells. Data are expressed as mean ± SEM. ** $p<0.01$, **** $p<0001$ by Student's t-test.

In contrast, no significant difference was observed in the percentage of eosinophils or macrophages between the anti-IL-4Rα treatment and the IgG isotype control groups (figure 3.6B and C). There were no significant differences in the percentage of neutrophils or lymphocytes

between the PBS-control and HDM control groups (figure 3.5D and E), or the anti-IL-4Rα-treatment and IgG isotype control groups (figure 3.6D and E).

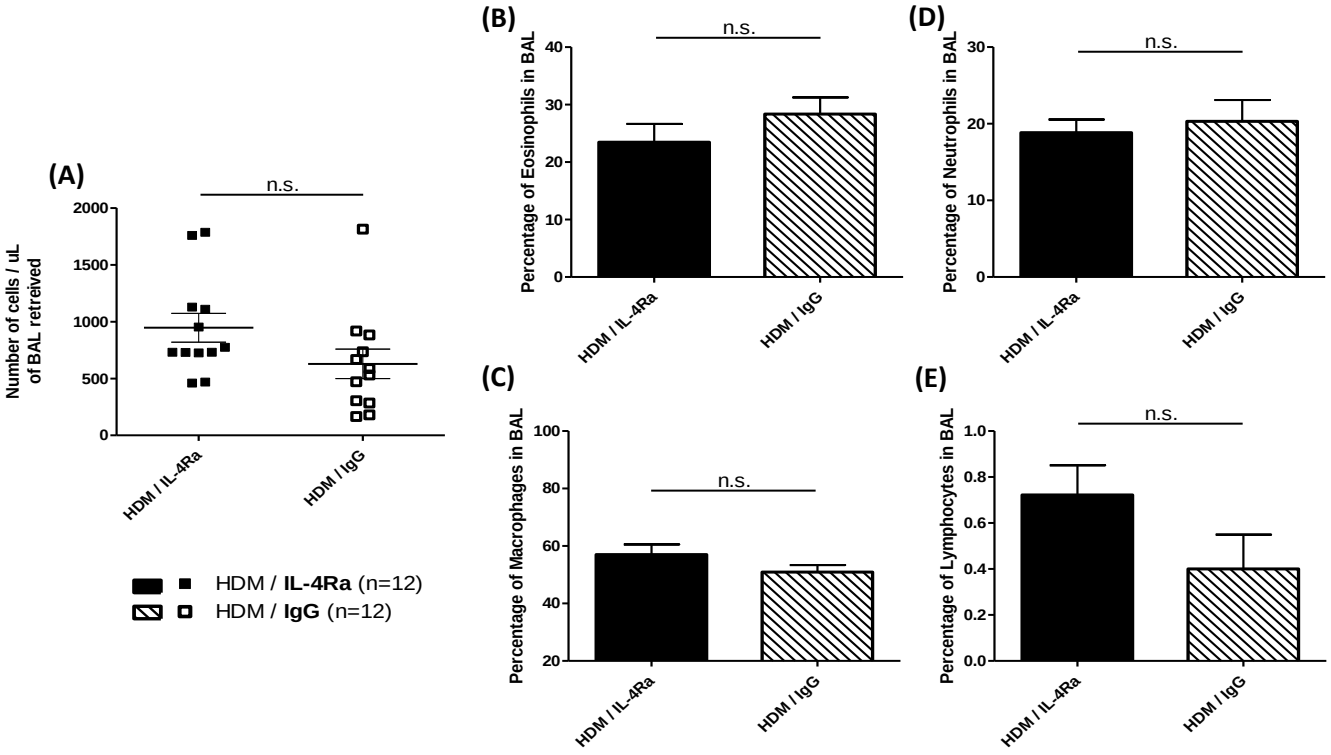

Figure 3.6 - BALF Cell Differentials in anti-IL-4Rα Treatment and IgG Isotype Control Groups

BALF was collected on day 8 p.i. from HDM-sensitized mice treated with either anti-IL-4Rα or IgG isotype control. (A) Cells were counted using a hemocytometer, and are expressed as the number of cells per microlitre of BALF retrieved. A cytospin was made from the cell pellet, and the percentage of (B) Eosinophils, (C) Macrophages, (D) Neutrophils, and (E) Lymphocytes was determined in a total of 200 counted cells. Data are expressed as mean ± SEM, and analyzed by (A,E) Mann-Whitney test and (B-D) Student's t-test.

3.3.3 Anti-IL-4Rα Treatment is Insufficient in Reducing Airway Goblet Cell Metaplasia

To assess levels of HDM-induced airway remodeling, a colour segmentation algorithm was applied on PAS-stained slides to visualize and quantify goblet cell metaplasia. Results were normalized to the length of basement membrane to account for differences in the size of the airways analyzed. In accordance with our findings from chapter 2, we found HDM-control mice

displayed significantly higher levels of PAS staining compared with PBS-control mice (figure 3.7 A-C). However, anti-IL-4Rα treated and IgG isotype control mice displayed similar levels of PAS staining (figure 3.7 D-F)

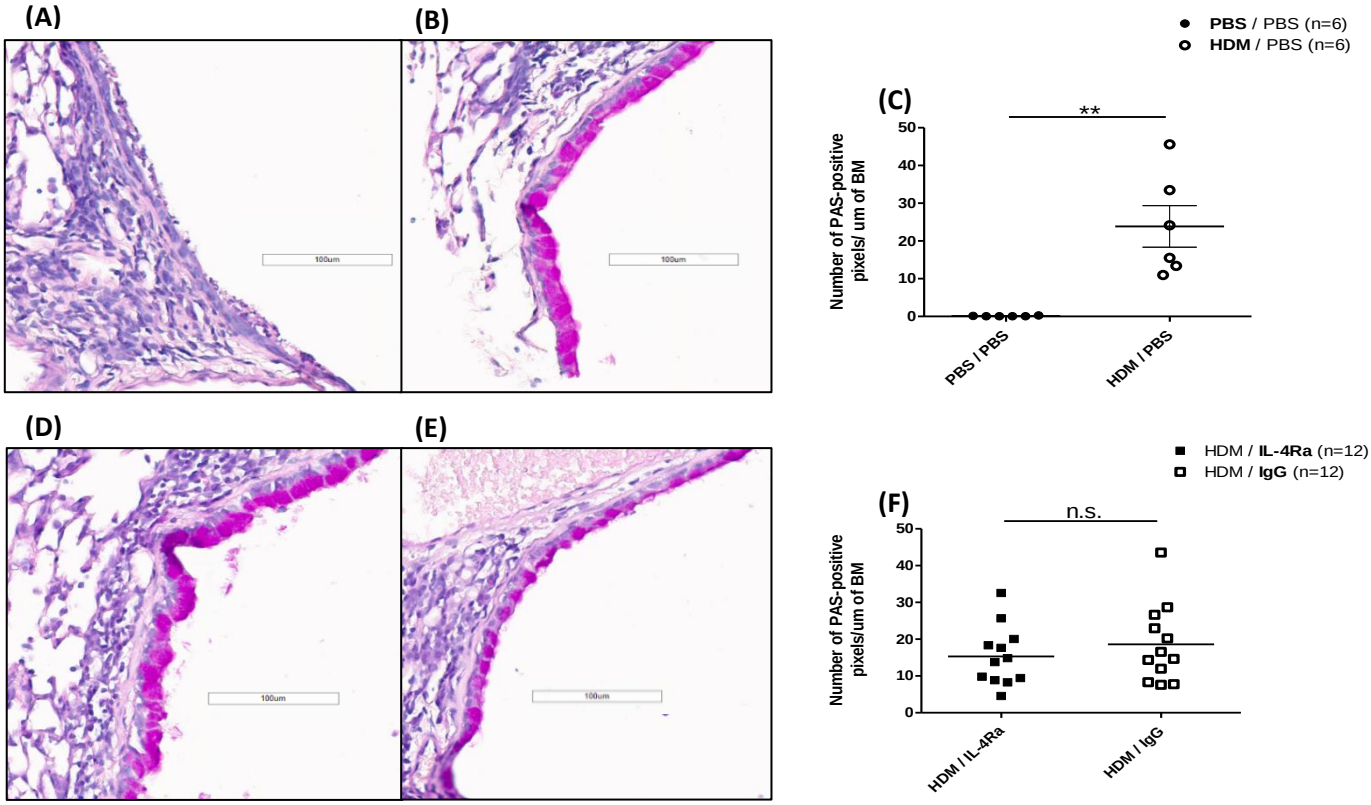

Figure 3.7 – Anti-IL-4Rα Treatment is Insufficient in Reducing HDM-induced Airway Goblet Cell Metaplasia

Representative images of PAS-stained tissues from the left lobe for (A) PBS-control, (B) HDM-control, (D) anti-IL-4Rα treatment, and (E) IgG isotype control groups. (C, F) A colour segmentation algorithm was used to quantify PAS-positively stained cells. Data are expressed as mean ± SEM. ** $p<0.01$ by Student's t test.

3.3.4 Cytokine Profile and pH1N1-specific IgG Following Anti-IL-4Rα Treatment

To interrogate changes in cytokine production induced by anti-IL-4Rα treatment, a multiplex assay and ELISA were performed on the BALF. Although there was a trend towards lower IFN-γ levels in HDM-control group, these differences were not significantly lower than IFN-γ levels in the PBS-control group (figure 3.8A). Anti-IL-4Rα treatment and IgG isotype

control groups also presented similar levels of BALF IFN-γ (figure 3.8B). Moreover, PBS-control and HDM-control mice displayed no significant difference in IL-4, IL-5, IL-17A (figure 3.8 C,E,G), or IFN-β BALF protein levels (figure 3.9A). In contrast, BALF from anti-IL-4Rα treatment group displayed significantly elevated IL-4, IL-5, and IL-17A (figure 3.8 D,F,H), and significantly reduced IFN-β levels (figure 3.9B) compared with BALF from IgG isotype control group.

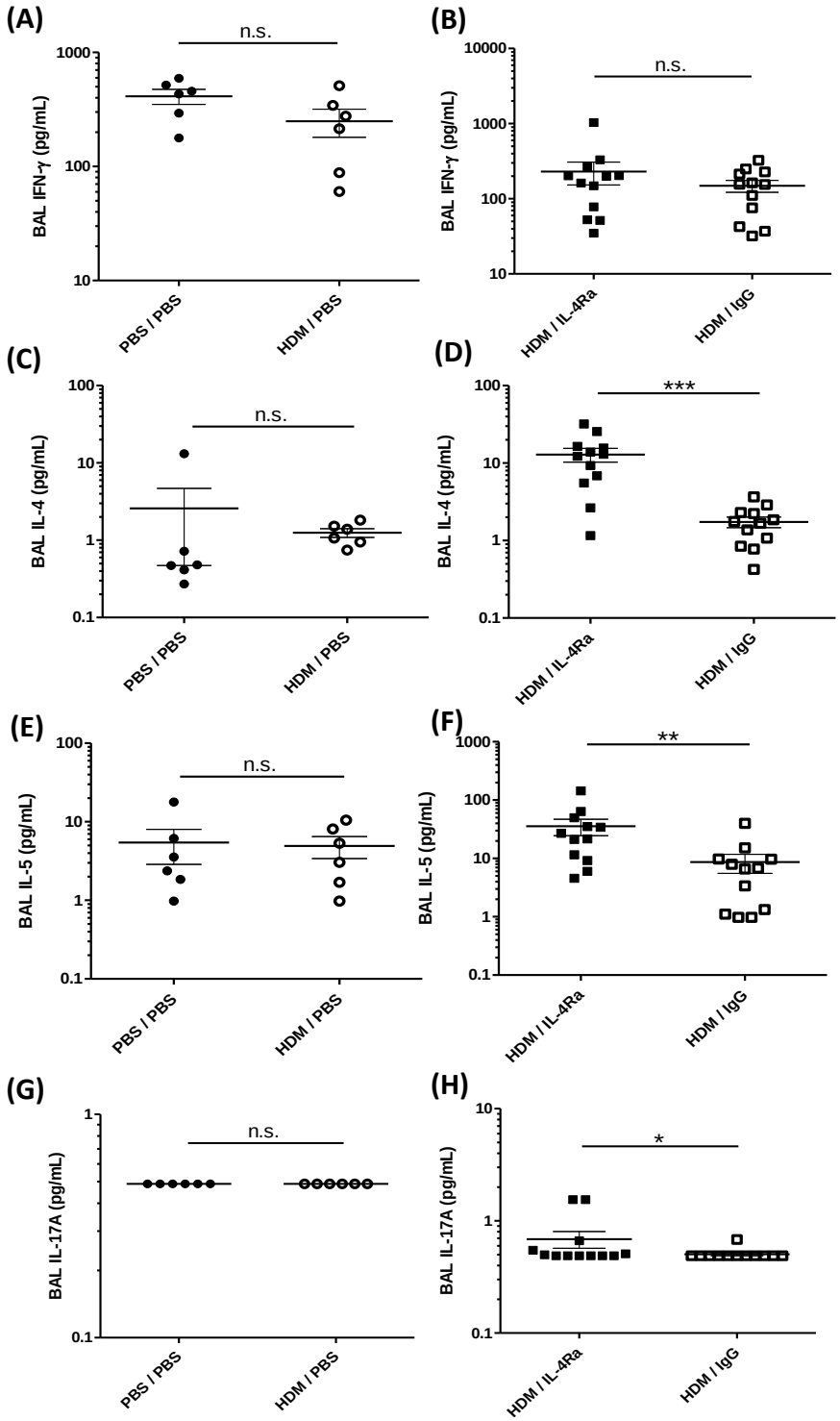

- **PBS** / PBS (n=6)
- **HDM** / PBS (n=6)
- HDM / **IL-4Ra** (n=12)
- HDM / **IgG** (n=12)

Figure 3.8 – Anti-IL-4Rα Treatment Results in Elevated BALF IL-4, IL-5, and IL-17A Protein Levels

BALF was collected from the right lobe. (A-B) IFN-γ, (C-D) IL-4, (E-F) IL-5, and (G-H) IL-17A protein levels were quantified using a multiplex assay. Data are expressed as mean ± SEM. *p<0.05, **p<0.01, ***p<0.001 by (A-E,G) Student's t test and (F,H) Mann-Whitney Test.

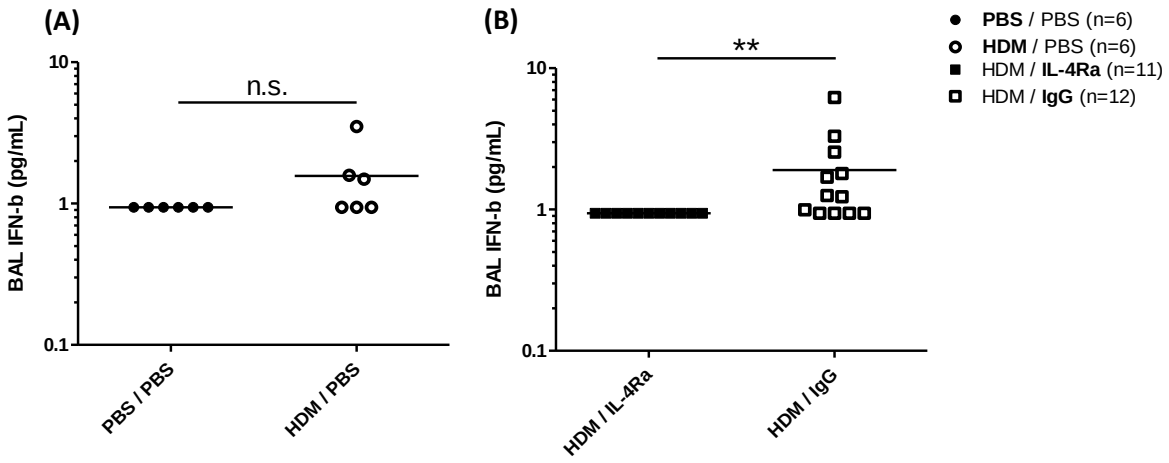

Figure 3.9 – Anti-IL-4Rα Treatment Group Present Lower BALF IFN-β Protein Levels
BALF was collected from the right lobe, and IFN-β protein levels were measured using ELISA. Data are expressed as mean ± SEM. **p<0.01 by (A) Student's t test and (B) Mann-Whitney Test.

To assess the level of acquired immunity to pH1N1, an in-house ELISA was developed to measure BALF IgG antibodies specific to the pH1N1 HA antigen. BALF collected from pH1N1-infected mice (positive control) showed significantly higher Optical Density (OD) associated with higher pH1N1-specific IgG concentration, as compared with BALF from non-infected mice (negative control – figure 3.10A). Furthermore, PBS-control group presented lower pH1N1-specific IgG than HDM-control group (figure 3.10B). In contrast, anti-IL-4Rα treatment group presented higher BALF pH1N1-specific IgG compared with IgG isotype control group (figure 3.10C).

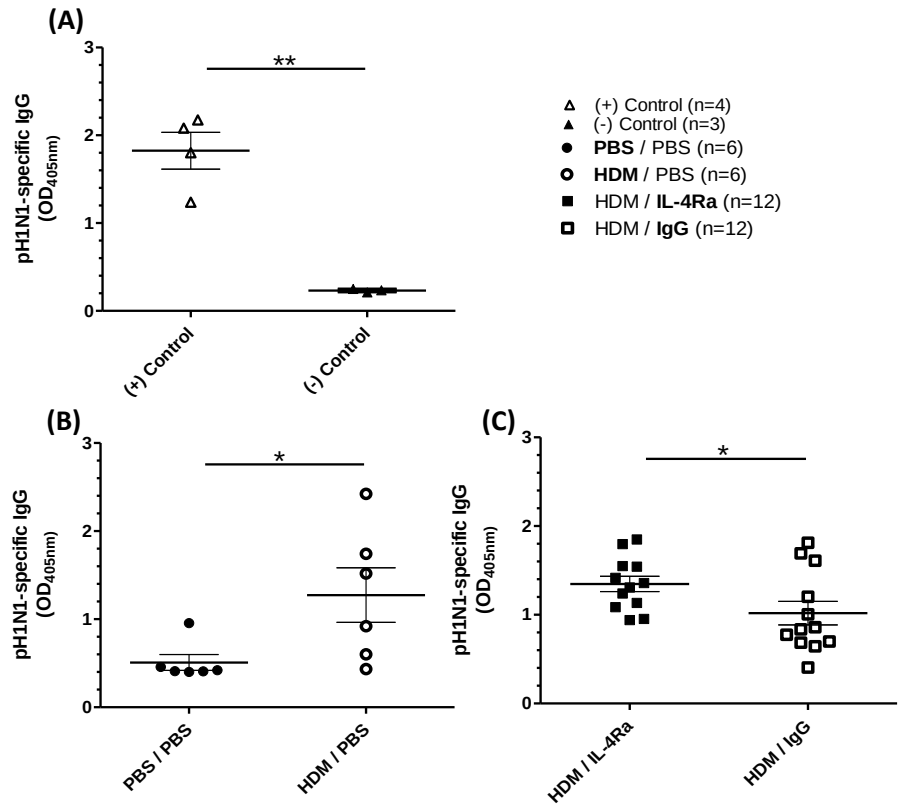

Figure 3.10 – Anti-IL-4Rα Treatment Group Present Elevated Levels of BALF pH1N1-specific IgG
BALF was collected from the right lobe, and levels of anti-pH1N1 IgG were measured using an in-house ELISA. (A) BALF from virus-infected and non-infected mice was used as positive and negative controls respectively, (B-C) BALF from treatment and control mice were measured at optical density (OD) 405. Data are expressed as mean ± SEM. *p<0.05, **p<0.01 by Student's t test.

3.4 Discussion

A vast amount of literature has supported the role IL-4Rα signaling as a potential mechanism for the induction and maintenance of allergic asthma. Furthermore, pre-clinical and clinical studies have demonstrated that IL-4Rα blockade abrogates some of the hallmark phenotypes of asthma, including eosinophilia and goblet cell metaplasia [168,169]. However, it has yet to be determined whether IL-4Rα has a role in modulating the level of virus-induced morbidity. We hypothesized that IL-4Rα blockade could be used in an established pH1N1 infection to reduce excessive morbidity in HDM-sensitized mice.

Similar to our findings from chapter 2, our results indicate that HDM-sensitized control mice experience significantly greater weight loss and higher viral loads than PBS-control mice.

To determine the role of IL-4Rα in HDM-induced excessive morbidity, we introduced the anti-IL-4Rα treatment on days 1 and 6 following an established pH1N1 infection. Our results indicate a significant reduction in weight loss on days 5-8 p.i. in HDM-sensitized mice that received anti-IL-4Rα treatment (HDM / anti-IL-4Rα). To elucidate the mechanism leading to reduced weight loss, qPCR was performed to measure viral load in homogenized lung tissue. We demonstrated that the anti-IL-4Rα treatment group present lower number of viral copies than the IgG isotype control group, pointing to lower viral burden as a potential mechanism implicated in reduced pH1N1-mediated morbidity. Interestingly, while anti-IL-4Rα treatment group experienced reduced weight loss compared with the IgG-isotype control group, anti-IL-4Rα treated mice lost significantly more weight than PBS-control mice. This indicates that anti-IL-4Rα treatment in an established pH1N1-infection is insufficient in reducing HDM-mediated excessive weight loss back to baseline levels. However, we found no significant difference in levels of viral titre between the anti-IL-4Rα treatment and PBS-control groups, indicating that the timing of the treatment strategy is sufficient to reduce viral burden.

Consistent with our results from chapter 2, HDM-control mice presented greater levels of PAS staining indicative of goblet cell metaplasia, as well as a greater percentage of eosinophils in BALF. The BALF cell differentials also revealed a reduction in the percentage of BALF macrophages in HDM-control mice, while the percentage of BALF neutrophils and lymphocytes, as well as the total concentration of BALF cells remained unchanged between the HDM-control and PBS-control groups. Although there was a trend towards lower BALF IFN-γ levels upon HDM sensitization, there was no significant difference between HDM-control and PBS control mice.

Previous studies have reported that IL-4Rα blockade reduces BALF eosinophilia and goblet cell metaplasia [169]. However, we were unable to reproduce these findings, and there was no significant difference between the anti-IL-4Rα treatment and the IgG isotype control groups in the level of PAS staining, the percentage of BALF eosinophils, macrophages, neutrophils, lymphocytes, or the total concentration of BALF cells. However, Hirota et al. introduced the anti-IL-4Rα intervention at the time of initial sensitization, and continued intervention throughout the sensitization protocol [169]. In contrast, we introduced the IL-4Rα blockade after 2 weeks of continuous sensitization, allowing effective establishment of allergic sensitization. Hence, differences observed in the level of goblet cell metaplasia and BALF eosinophil percentage between the two studies may be due to differences in the experimental design.

To characterize the immune profile of mice in each group, BALF samples were tested using an array of ELISAs and Multiplex assays. IFN-β was used as a marker of innate immunity. Previous studies using bronchial epithelial cells from asthmatic patients have reported 2.5 fold lower levels of RV-induced IFN-β than healthy controls, which correlated with an increase in RV replication and release [150]. In our study however, we did not find a significant difference in BALF IFN-β levels between the PBS-control and HDM-control groups. Another study reported attenuation of RV-induced IFN-β response by respiratory epithelial cells upon treatment with IL-4 and IL-13 [179]. While we expected an increase in IFN-β levels when the signaling of IL-4 and IL-13 was blocked through the anti-IL-4Rα treatment, our findings indicated that mice receiving the IL-4Rα blockade had lower levels of BALF IFN-β than IgG isotype controls. The inconsistencies found may be attributed to the time of IFN-β measurement; Wark et al. and Contoli et al. measured IFN-β after 8, 24, and 48 hours incubation, with RV and IL4/IL-13

respectively [150,179]. In contrast, we measured BALF IFN-β levels 8 days after pH1N1 infection. Hence, while the literature may suggest asthmatics have delayed induction of IFN-β production, studies have yet to investigate the maintenance of IFN-β production following pH1N1 infection. Our study suggests that mice receiving IgG isotype control are able to sustain IFN-β production for a longer period of time, which may be attributed to having elevated viral loads on day 8 post-infection.

BALF IL-4 and IL-5 levels were measured as indicators of the Th_2 response. While other studies have reported increased BALF levels of these cytokines upon OVA sensitization, we found no significant difference in BALF IL-4 and IL-5 levels between PBS-control and HDM-control mice [180]. However, protein levels of both of these cytokines were elevated in the anti-IL-4Rα treatment group compared with the IgG isotype control group. An inability of IL-4 to signal through IL-4Rα may contribute to this cytokine's low consumption, thus leading to its accumulation in BALF. However, Tomkinson et al. reported lower protein levels of IL-4 and IL-5 in OVA challenged mice treated with an IL-4Rα antagonist [181]. Differences in our findings may potentially be due to differences in experimental design, and be attributed to the use of pH1N1 infection in our model.

IL-17A has been implicated in the pathogenesis of severe asthma, and several studies have identified elevated levels of this cytokine in bronchial biopsies, BALF, and sputum of subjects with asthma [182-184]. Furthermore, IL-17A has been shown to induce airway mucous cell metaplasia through a STAT6-independent pathway [185]. Although we found no difference in BALF IL-17A levels between the PBS-control and HDM-control samples, the level of this cytokine were below the detection limit of the multiplex assay we used. Hence, differences in the levels of this cytokine between control groups may be masked due to experimental shortcomings,

and a more sensitive assay is required for accurate detection of this cytokine. Although we were unable to detect levels of this cytokine in several of our samples, there seems to be a significant increase in BALF IL-17A levels of anti-IL-4Rα treatment group when compared with the IgG isotype control group. Previous studies have reported that STAT6 knockout mice have elevated BALF IL-17A protein levels upon OVA challenge, consistent with our findings [185]. Although the exact mechanism has yet to be elucidated, it seems that blockade of IL-4Rα or downstream STAT6 blockade results in increased production of IL-17A.

Lastly, we measured pH1N1-specific IgG levels in BALF as an indicator of the virus-specific humoral response. We found that HDM-control mice presented elevated levels of pH1N1-specific IgG, compared with PBS-control mice. Interestingly, the anti-IL-4Rα treatment group displayed elevated levels of pH1N1-specific IgG when compared with the IgG isotype control group, pointing to an enhancement in the humoural response upon blockade of IL-4Rα signaling. A previous study also found elevated levels of serum RSV-specific IgG2A in mice treated with an IL-4Rα antisense oligonucleotides [186]. The mechanism whereby IL-4Rα blockade increases IgG production has yet to be elucidated.

Our data supports the hypothesis that IL-4Rα blockade reduces pH1N1-mediated morbidity in HDM-sensitized mice through a mechanism that reduces viral load. This finding emphasizes the importance of Th_1/Th_2 balance in the context of asthma exacerbations, and how alterations in this tightly regulated response could have a considerable impact in health and disease. We have been able to identify IL-4Rα blockade as not only a method to reduce asthma-associated symptoms, but as an effective treatment for viral-induced morbidity in the form of weight loss in sensitized mice.

Chapter 4: Early and Systematic IL-4Rα Blockade Prevents pH1N1-mediated Weight Loss in a Mouse Model of Allergic Asthma

4.1 Introduction

Vaccinations are currently the principal method for the prevention of influenza-mediated morbidity and mortality [24]. However, from the time a new strain of influenza with pandemic potential is identified, it may take 6 months for a vaccine to be developed [16]. In the case of the 2009 pandemic, the first case of H1N1 was reported in Mexico in April, while the deployment of vaccines did not begin until September [187]. During this period, CDC reported over 37,000 cases of laboratory-confirmed H1N1 in the United States alone. This period of waiting without suitable prevention strategies can have a devastating effect on the vulnerable population [188]. An alternative method of prevention that can be deployed quickly needs to be developed to address the needs of individuals with comorbidities and risk factors, such as the asthmatic population.

Our results from Chapter 3 indicate a significant improvement in the symptoms of sensitized mice treated with anti-IL-4Rα. However, it is unknown whether IL-4Rα blockade could be used as a preventative intervention. We hypothesized that early and systematic blockade of IL-4Rα signaling could reduce morbidity in the form of weight loss in HDM-sensitized mice.

4.2 Methods

Animal Experimental Protocol

As described in previous chapters, 6-8 week old male BALB/c mice (Jackson Laboratories, Bar Harbour, MA) were intranasally sensitized with HDM (*Dermatophagoides pteronyssinus*, 25ug of protein in 35uL of sterile PBS) on a daily basis [139]. Intranasal HDM/PBS exposure was performed on days -12 to -8, and days -5 to -1 prior to- and on days 2 to 7 following- viral infection. A single dose of pH1N1 (50ul, $10^{6.4}$ EID_{50}/mL) was intranasally instilled on day 0 (figure 4.1).

Anti-IL-4Rα (4-3, hybrid IgG1) and IgG1 (4G8) monoclonal antibodies were obtained from Amgen (Seattle, WA), and 2 mg of each antibody diluted in PBS was administered intraperitoneally per respective animal group, as previously described [174]. The volume of PBS used for the delivery of the antibodies was based on 10uL of PBS per gram of mouse weight. IP injections were performed on days -12, -7, and -2 prior to- and day 3 following- viral infection to create a preventative intervention model. Animal health status and weight were monitored daily, and mice were sacrificed on day 8 p.i. to perform outcome measurements (figure 4.1).

Two groups of animals were studied: (1) anti-IL-4Rα (preventative) intervention (IN HDM / IP anti-IL-4Rα), and (2) IgG isotype-control (IN HDM / IP IgG).

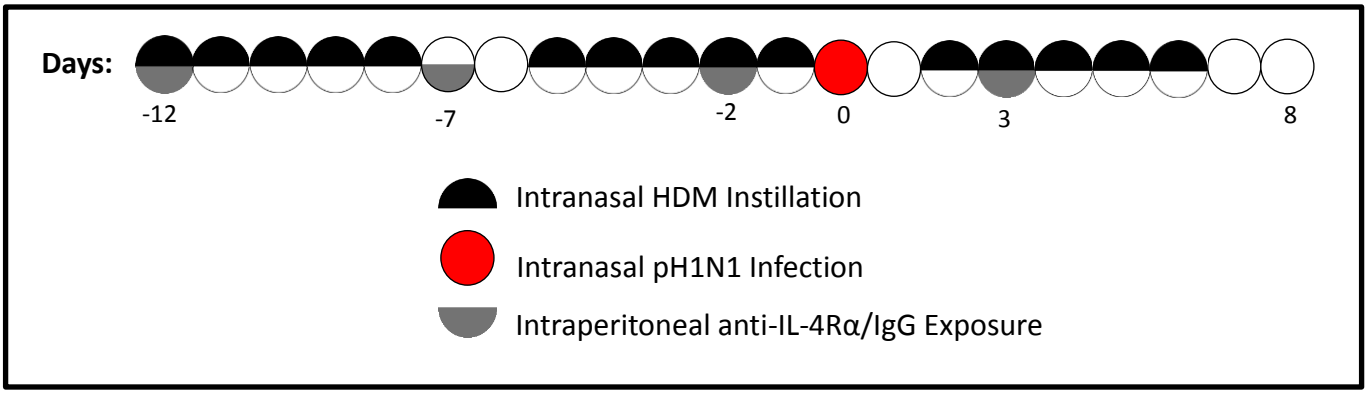

Figure 4.1 – Anti-IL-4Rα Preventative Intervention Experimental Protocol
IN HDM instillations were performed 5 days per week, for 3 consecutive weeks (marked black). IN pH1N1 inoculation was performed on day 0 (marked red), and IP IL-4Rα/IgG injections were performed on days -12, -7, and -2 prior to pH1N1 infection, and day 3 following pH1N1 infection (marked gray).

Ethics Statement

All work was carried out in accordance with protocols approved by the University of British Columbia Animal Care and Biosafety Committees (A16-0331 and B17-0007).

Tissue Harvest Sample processing

BALF collection and protein detection, right lobe homogenization and RNA extraction, left lobe histology and morphometry measurements, as well as viral load quantification were performed as previously described in chapters 2 and 3.

Statistical analysis

Weight loss was compared using two-way ANOVA with a Bonferroni correction for multiple testing. All other parameters were tested for normality using the D'Agostino & Pearson omnibus normality test. Parameters that were not normally distributed ($p < 0.05$), namely BALF total cell concentration and neutrophil differentials, as well as BALF IFN-β levels were analyzed using the Mann-Whitney U test. All other parameters passed the normality test, and were analyzed using a two-tailed Student's t-test. Data are expressed as mean ± SEM, and p-values

<0.05 were considered significant. All statistical analysis was performed using GraphPad Prism version 5 (La Jolla, CA).

4.3 Results

4.3.1 Anti-IL-4Rα Preventative Intervention Reduces H1N1-mediated Morbidity in HDM-sensitized Mice

In order to determine the role that an early IL-4Rα blockade intervention would have on pH1N1-mediated morbidity, mice were weighed throughout the course of the experiment. Our results indicate that an early anti-IL-4Rα intervention (IN HDM/ IP anti-IL-4Rα) significantly reduces weight loss on days 6-8 p.i. (figure 4.2A), compared with mice receiving IgG isotype control (IN HDM/ IP IgG). To examine the role of IL-4Rα blockade on viral load, qPCR was performed on the lung homogenate to determine the number of viral copies. The anti-IL-4Rα intervention group presented significantly lower number of viral copies than the IgG isotype control group (figure 4.2B).

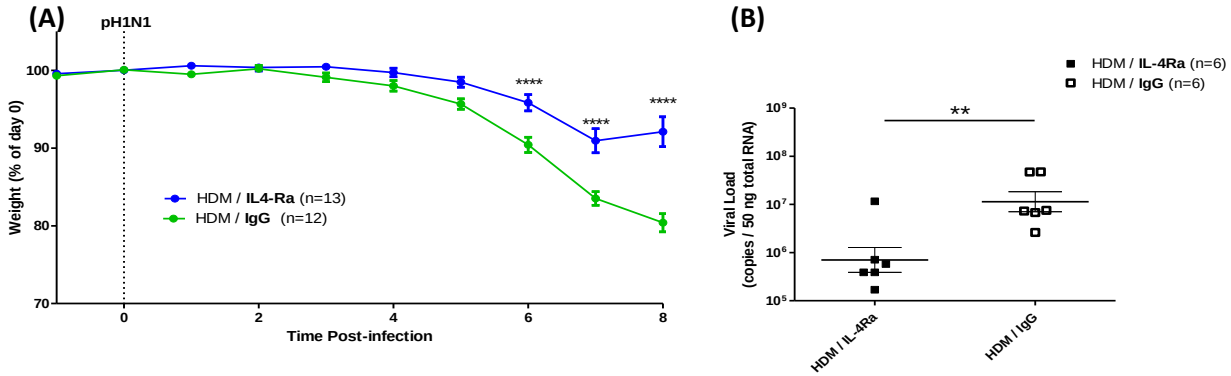

Figure 4.2 – Anti-IL-4Rα Preventative Intervention Reduces pH1N1-mediated Excessive Weight Loss and Viral Load in HDM-sensitized Mice

Mice were intranasally exposed to HDM for 3 weeks, and IP injected on days -12, -7, -2, and 3 pi with either anti-IL-4Rα or IgG isotype control. (A) Mice were weighed daily, and the mean change in body mass is plotted as a percentage of weight on day 0. Data represent two independent experiments, and were analyzed using two-way ANOVA with a Bonferroni correction. (B) Viral load was quantified using qPCR on the homogenized right lobe, and is expressed as the number of copies per 50ng of total RNA. Data were analyzed using Student's t-test, and are expressed as mean ± SEM. ** p<0.01, **** p<0.0001

4.3.2 IL-4Rα Preventative Intervention Reduces the Percentage of BALF Eosinophils

We sought to determine whether early and intermittent IL-4Rα blockade could modify BALF immune cell changes caused by HDM-sensitization. While there were no significant changes in the overall concentration of immune cells in BALF retrieved (figure 4.3A), we found that anti-IL-4Rα intervention could significantly reduce the percentage of BALF eosinophils (figure 4.3B). Furthermore, anti-IL-4Rα intervention group presented a higher percentage of BALF macrophages (figure 4.3C) compared with IgG isotype control group, while there were no significant differences in the percentage of neutrophils (figure 4.3D) or lymphocytes (figure 4.3E).

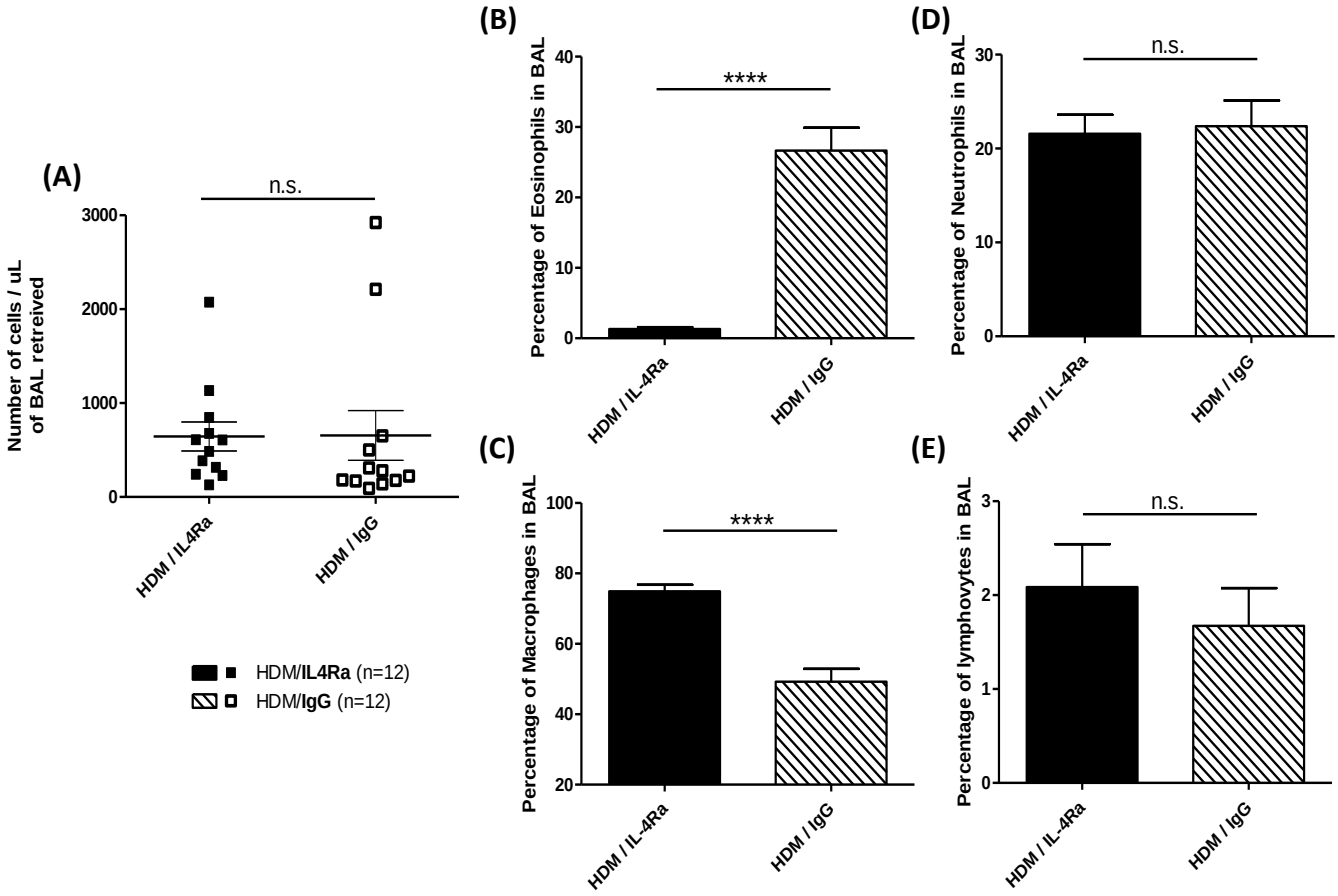

Figure 4.3 – Anti-IL-4Rα Preventative Intervention Reduces the Percentage of Eosinophils and Restores the Percentage of Macrophages in BALF

BALF was collected on day 8 p.i. from HDM-sensitized mice receiving either anti-IL-4Rα or IgG isotype control. (A) Cells were counted using a hemocytometer, and are expressed as the number of cells per micrlitre (uL) of BALF retrieved. A cytospin was made from the cell pellet, and the percentage of (B) Eosinophils, (C) Macrophages, (D) Neutrophils, and (E) Lymphocytes was determined in a total of 200 counted cells. Data are expressed as mean ± SEM. **** $p<0.0001$ by (A,D) Mann-Whitney test and (B, C, E) Student's t test.

4.3.3 Anti-IL-4Rα Preventative Intervention Reduces Airway Goblet Cell Metaplasia and Mucous Hypersecretion

To investigate the role of anti-IL-4Rα intervention in HDM-induced airway remodeling, a colour segmentation algorithm was used on PAS-stained slides to visualize and quantify goblet cell metaplasia. To account for variability in the size of airways analyzed, results were normalized to the length of basement membrane (um). Our results indicate that the anti-IL-4Rα intervention group presented a significant reduction in PAS staining (representative of goblet cell metaplasia) compared with IgG isotype control group (figure 4.4C).

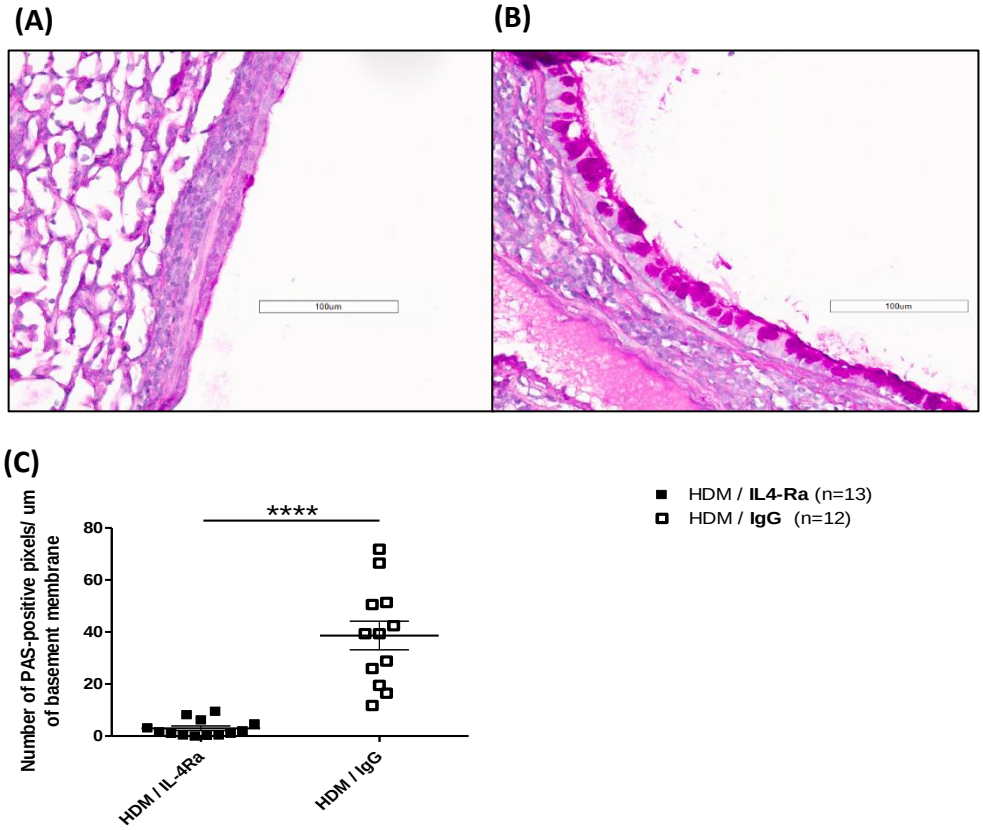

Figure 4.4 – Anti-IL-4Rα Preventative Intervention Reduces Airway Goblet Cell Metaplasia

Representative images of PAS-stained tissues from the left lobe for (A) Anti-IL-4Rα intervention, and (B) IgG isotype control mice. (C) A colour segmentation algorithm was used to quantify PAS-positively stained cells. Staining was normalized to the length of basement membrane. Data are expressed as mean ± SEM. **** $p<0.0001$ by Student's t test.

4.3.4 Cytokine Profile Following Anti-IL-4Rα Preventative Intervention

ELISA and multiplex assays were performed to interrogate changes in cytokine profile induced by anti-IL-4Rα intervention. No significant differences were found in the BALF protein levels of IFNγ, IL-4, or IL-5 (figure 4.5A, C, D), or in the levels of pH1N1-specific IgG concentration (figure 14.6B) between the anti-IL-4Rα intervention and the IgG isotype control groups. However, mice receiving the anti-IL-4Rα intervention presented significantly elevated protein levels of BALF IL-17A (figure 4.5B), and significantly lower levels of BALF IFN-β (figure 4.6A)

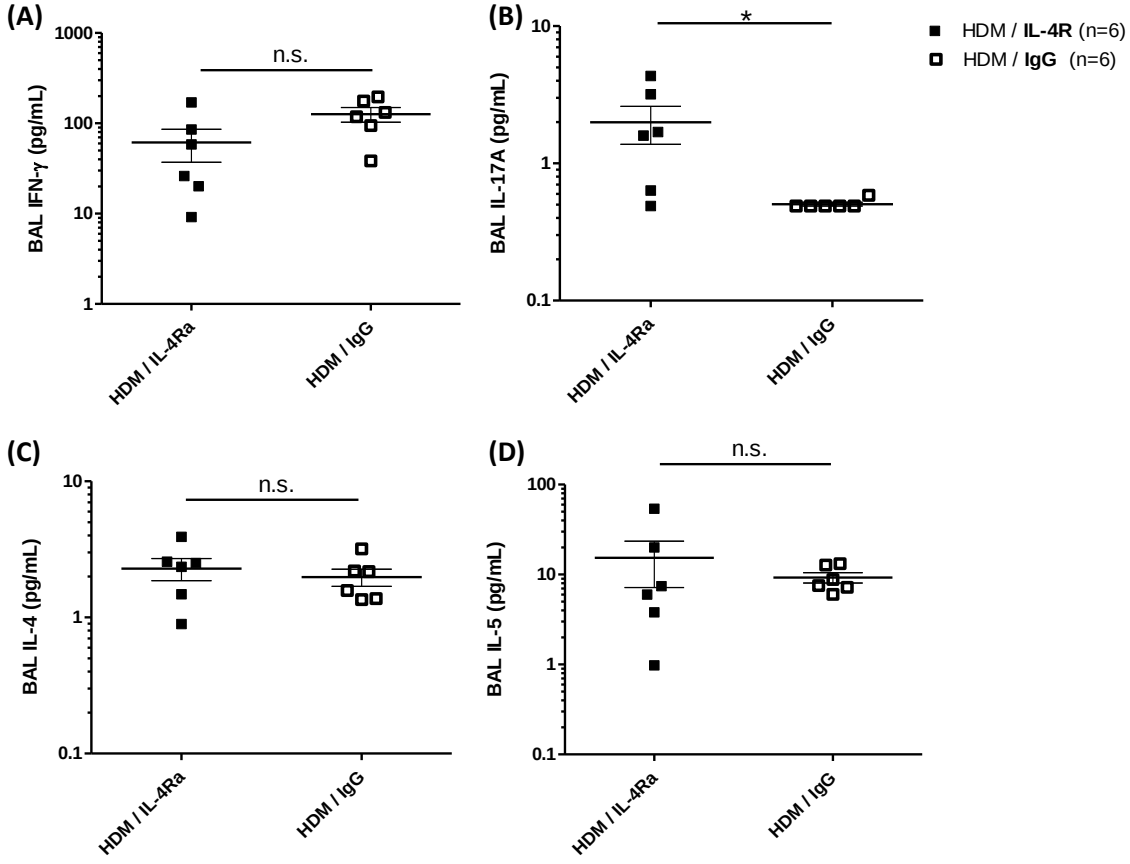

Figure 4.5 - BALF Cytokine Profile Following Anti-IL-4Rα Preventative Intervention
BALF was collected from the right lobe, and a multiplex assay was used to quantify protein levels of (A) IFN-γ, (B) IL-17A, (C) IL-4, and (D) IL-5. Data are expressed as mean ± SEM. *p<0.05 by Student's t test.

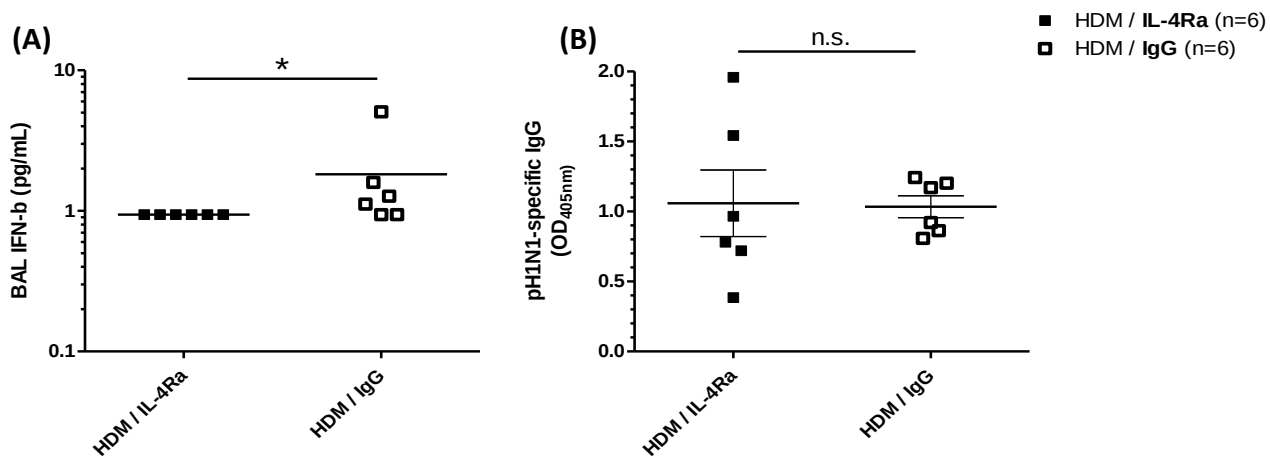

Figure 4.6 - BALF IFN-β and pH1N1-specific IgG Protein Levels Following Anti-IL-4Rα Preventative Intervention

BALF was collected from the right lobe. (A) IFN-β (Mann-Whitney Test), and (B) pH1N1-specific IgG (Student's t-test) levels were measured using ELISA. Data are expressed as mean ± SEM. *$p<0.05$.

4.4 Discussion

Although several studies have identified vaccinations as the most effective method of prevention during the 2009 H1N1 pandemic, the production and circulation of a vaccine takes at least 6 months [16]. Developing countries are at a greater risk due to having a highly vulnerable population and limited medical resources [189]. A prevention strategy that can be dispatched quickly needs to be implemented to protect vulnerable populations during this critical 6 month waiting period. We hypothesized that early and systematic IL-4Rα blockade could reduce pH1N1-associated morbidity in HDM-sensitized mice.

Consistent with our findings from chapters 2 and 3, significant weight loss was observed on days 5-8 following pH1N1 infection. However, our findings indicate that early and systematic blockade of IL-4Rα signaling significantly reduces weight loss. Moreover, anti-IL-4Rα intervention allowed mice to stabilize and start regaining weight between days 7-8 p.i., while IgG isotype control mice continued to lose weight. To assess the level of viral load between the

experimental groups, we measured the number of viral copies using qPCR. Interestingly, the anti-IL-4Rα intervention group presented significantly lower number of viral copies compared with the IgG isotype control group. Having lower a viral burden may serve to explain why the anti-IL-4Rα intervention group experienced reduced weight loss and morbidity.

We sought to determine whether early and intermittent IL-4Rα blockade influences airway immune cell profile or goblet cell metaplasia. Consistent with our previous results, we found no significant difference in the total concentration of cells in BALF, or the percentage of BALF neutrophils and lymphocytes. In contrast from our findings from the anti-IL-4Rα treatment design in chapter 3, our results indicate a significant reduction in the percentage of BALF eosinophils and the level of PAS staining in the anti-IL-4Rα preventative intervention design. We also found a significant increase in the percentage of BALF macrophages, which may be a result of the reduction in eosinophil recruitment to the airways upon anti-IL-4Rα intervention. These results point to the importance of the timing of the initiation of IL-4Rα blockade and the frequency of treatment in achieving a reduction in asthma characteristics. Our data indicating reduced BALF eosinophilia and goblet cell metaplasia are consistent with a previous study by Hirota et al., which also initiated the anti-IL-4Rα intervention early on and systematically during sensitization [169].

Using ELISA and multiplex assays, we measured an array of cytokines to profile the immune response within the airways. While there was a trend towards elevated levels of IL-4 and IL-5 in the anti-IL-4Rα intervention group, these differences were not significant. Our findings in chapter 3 however, indicated that anti-IL-4Ra treatment resulted in a significant increase in BALF IL-4 and IL-5. Differences in these findings may be attributed to having a lower number of replicates (n=6) in the preventative intervention design.

IFN-γ and IL-17A were measured as markers of Th_1 and Th_{17} response, respectively. While the anti-IL-4Rα intervention had no effect on BALF IFN-γ levels, it was associated with a significant increase in BALF IL-17A levels. These results are consistent with our findings from chapter 3, where IL-4Rα blockade as a treatment strategy also increased BALF IL-17A. Moreover, other studies have also reported STAT6 (downstream of IL-4Rα signaling) knockout mice present elevated BALF IL-17A following OVA challenge [185].

We measured IFN-β as a marker of the antiviral innate immunity. Interestingly, we found lower levels of BALF IFN-β in the anti-IL-4Rα intervention group than the IgG isotype control group. This was similar to our findings from chapter 3, whereby the anti-IL-4Ra treatment group had lower IFN-β levels than the associated IgG-isotype control group. One explanation may be that consistently elevated number of viral copies in IgG-isotope control group is facilitating the continuous production of IFN-β, leading to elevated levels of this cytokine in BALF. Lastly, we measured pH1N1-specific IgG as an indicator of virus-specific humoural response. We found no significant difference between the anti-IL-4Rα intervention and IgG isotype control groups.

Taken together, we have demonstrated early and intermittent IL-4Rα blockade as an effective preventative intervention in addressing pH1N1-mediated morbidity. Furthermore, our data implicate a reduction in asthma symptoms (eosinophilia and goblet cell metaplasia) as a potential mechanism whereby early IL-4Rα blockade prevents morbidity. Our findings could provide an alternative means to prevent morbidity in the vulnerable asthmatic population during the critical period when a pandemic virus is spreading but a vaccine has yet to be developed.

Chapter 5: Discussion

5.1 Conclusion

The 2009 H1N1 pandemic took the lives of at least 18,500 people worldwide, and placed a significant burden on the healthcare system [70]. However, individuals previously diagnosed with asthma experienced the greatest adverse health outcomes, and several studies reported asthma as a significant risk factor for pH1N1-associtaed hospitalization and morbidity [73,75]. The aim of our study was to examine the asthmatic immune response to pH1N1, and investigate potential therapies that may be used to alleviate pH1N1-mediated morbidity and mortality in the asthmatic population.

Allergic asthma is generally characterized through a Th_2-skewed phenotype, with an over production of IL-4, IL-5, and IL-13. These cytokines have been implicated in the establishment of some of the hallmarks of asthma including airway remodeling and eosinophilia [118,120,121]. Furthermore, Th_2 cytokines are able to inhibit Th_1 cell polarization and their antiviral function [127-129]. We hypothesized that a constitutively skewed Th_2 phenotype in asthmatics may reduce their ability to mount an effective antiviral Th_1 response, hence resulting in the increased morbidity and mortality observed during the 2009 H1N1 pandemic. In chapter 2, we aimed to create a model of allergic asthma that we could utilize to test this hypothesis. Similar to humans, we found that sensitized mice experienced greater morbidity in the form of greater weight loss and elevated viral titres 8 days following pH1N1 infection. Furthermore, sensitized mice exhibited lower levels of IFN-γ and higher levels of IL-13. Most importantly, we were able to develop a model of allergic asthma and pH1N1 infection that is clinically relevant to the 2009 pandemic, and may be used to investigate potential therapies to protect the vulnerable asthmatic population against a future pandemic IAV strain.

Currently, antivirals including neuraminidase inhibitors and adamantes are the only available option for the treatment of IAV infection. However, clinicians are often unable to use antiviral drugs due to resistance conferred by the virus [21]. Furthermore, the effectivity of antivirals significantly decreases 48 hours following the initial infection [25,26]. Hence, many individuals who had contracted pH1N1 during the pandemic, including asthmatics who were at a greater risk of experiencing adverse health outcomes, had few treatment options available. In chapter 3, we sought to investigate the role of Th_2 cytokine signaling blockade as a potential treatment method. Using the murine model developed in the previous chapter, we treated sensitized mice following pH1N1 infection with a monoclonal antibody that would prevent IL-4Rα signaling. We found that IL-4Rα blockade was effective in reducing weight-loss and viral burden in an established pH1N1 infection. However, reduction in weight loss and viral titre were not associated with a reduction in asthma characteristics, and sensitized mice continued to present elevated BALF eosinophils and airway goblet cell metaplasia following IL-4Rα blockade.

Vaccinations have proved to be the most effective method of prevention against both seasonal and pandemic IAV strains. However, vaccines take at least 6 months to be developed and distributed from the time an IAV strain is identified [16]. During this time, an IAV with pandemic potential can quickly disseminate through the population, taking the lives of vulnerable individuals. Hence, limiting viral spread and reducing the risk of adverse health outcomes is critical during this initial 6 month period while the vaccine is being developed. However, there is a lack of pharmaceutical interventions that reduce the level of health complications in individuals at risk of contracting the pandemic strain. We hypothesized that early and systematic blockade of IL-4Rα could prevent morbidity following pH1N1 infection in

sensitized mice. Our results indicated a significant reduction in pH1N1-mediated weight loss and reduced viral burden upon IL-4Rα blockade. Furthermore, early and systematic IL-4Rα blockade was associated with a reduction in BALF eosinophils and airway goblet cell metaplasia, which may be occurring a result of introducing this intervention early on during sensitization.

Historical records indicate the occurrence of IAV pandemics every 10-40 years. With over 9 years since the 2009 H1N1 pandemic, we are due for another pandemic in the near future. A growing body of literature suggests a complex interplay in the host-virus interaction when a new strain of virus is encountered, such as it was during the H1N1 pandemic. Our study contributes to this by demonstrating the importance of Th_1/Th_2 balance during viral infections. Furthermore, we have been able to demonstrate an important role for IL-4Rα blockade that may be utilized to address adverse health outcomes by reducing the severity of disease against a pandemic IAV strain in atopic individuals. In the face of a potential influenza pandemic in the next 10-30 years, our findings could be utilized to protect the vulnerable asthmatic population.

5.2 Limitations and Future Directions

The utilization of animal models has a played a key role in human disease research, and has helped us gain a better understanding of the pathogenesis of asthma. However, careful consideration of associated limitations need to be addressed before translating findings into clinical practice. Although the HDM-sensitization model utilized in this study has demonstrated a strong allergic component similar to human Th_2-driven allergic asthma, studies have reported a much weaker serum IgE response in mice. Furthermore, the line between allergen sensitization and allergen challenge may be blurred when the model involves repeated HDM exposure [190].

While our study identified IL-4Rα blockade as an effective method in reducing pH1N1-mediated morbidity in sensitized mice, we have yet to elucidate its effect on the downstream signaling cascade. A number of studies have reported a reduction in the phosphorylation and thus activation of STAT6 upon IL-4Rα blockade [169,191]. STAT6 is a transcription factor that can mitigate the signal for IL-4 and IL-13, thereby inducing some of the characteristics of asthma [192]. Hence, a reduction in STAT6 phosphorylation upon IL-4Rα blockade may indicate a reduction in Th_2 cytokine effector function, and thus Th_2 skewing. However, IL-4Rα signaling can also activate IRS-2, resulting in subsequent signaling leading to the activation of the PI3K pathway [193]. While The IRS-2/PI3K pathway has been described to provide mitogenic and anti-apoptotic signals to sustain the Th_2 response, it can also contribute towards Th_2 differentiation and skewing [194,195]. However, it has yet to be determined whether IL-4Rα blockade can reduce IRS-2 activation and downstream signaling. Measurements of STAT6 phosphorylation and the level of PI3K activity may provide further insight regarding the downstream activity of IL-4Rα blockade and the mechanism involved in the reduction of pH1N1-mediated morbidity in sensitized mice.

Although we have demonstrated a significant role for IL-4Rα blockade in both protecting and treating the vulnerable asthmatic population during an IAV pandemic, it is unclear how this intervention could benefit the general population. The question remains as to whether blockade of Th_2 skewing could boost the antiviral response, and hence reduce the level of morbidity and mortality in individuals without asthma. Additional experiments using non-sensitized mice infected with pH1N1 would be necessary to determine how IL-4Rα blockade could benefit non-atopic individuals.

While the H1N1 pandemic caused significant morbidity and mortality in the asthmatic population, other viruses cause more frequent infections and are of a more immediate concern to address. RV infections cause upper respiratory infection, and account for 80% of asthma exacerbations in adults [196]. Respiratory syncytial virus (RSV) is another virus that causes lower respiratory infections, and causes a substantial number of exacerbations in asthmatic children [197]. Considering the healthcare costs associated with RV and RSV-induced exacerbations, it would be valuable to determine whether IL-4Rα blockade could reduce associated exacerbation symptoms and thus shorten the duration of hospitalization.

Avian influenza infection in humans generally affects the lower respiratory tract and occurs sporadically as a result of exposure to poultry. The avian influenza H7N9 was first identified in 2013, and has since caused an epidemic in China with other 1336 laboratory-confirmed cases. While H7N9 infection is sporadic and there is a low level of human-to-human transmission, it is highly pathogenic, and the case fatality rate is estimated to be around 40% [198,199]. Furthermore, the H7N9 virus has conferred neuraminidase inhibitor resistance, leaving few treatment options available for infected individuals [200,201]. Determining the treatment potential of IL-4Rα blockade against the H7N9 IAV strain could provide valuable information that may be utilized to contain the current epidemic.

References

1. Sellers SA, Hagan RS, Hayden FG, Fischer WA, 2nd. The hidden burden of influenza: A review of the extra-pulmonary complications of influenza infection. *Influenza Other Respir Viruses*, 11(5), 372-393 (2017).
2. Thommes EW, Kruse M, Kohli M, Sharma R, Noorduyn SG. Review of seasonal influenza in Canada: Burden of disease and the cost-effectiveness of quadrivalent inactivated influenza vaccines. *Hum Vaccin Immunother*, 13(4), 867-876 (2017).
3. Molinari NA, Ortega-Sanchez IR, Messonnier ML *et al.* The annual impact of seasonal influenza in the US: measuring disease burden and costs. *Vaccine*, 25(27), 5086-5096 (2007).
4. Taubenberger JK, Morens DM. The pathology of influenza virus infections. *Annual review of pathology*, 3, 499-522 (2008).
5. Ozawa M, Kawaoka Y. Cross talk between animal and human influenza viruses. *Annu Rev Anim Biosci*, 1, 21-42 (2013).
6. Webster RG, Yakhno M, Hinshaw VS, Bean WJ, Murti KG. Intestinal influenza: replication and characterization of influenza viruses in ducks. *Virology*, 84(2), 268-278 (1978).
7. Stevens J, Blixt O, Glaser L *et al.* Glycan microarray analysis of the hemagglutinins from modern and pandemic influenza viruses reveals different receptor specificities. *J Mol Biol*, 355(5), 1143-1155 (2006).
8. Wikramaratna PS, Sandeman M, Recker M, Gupta S. The antigenic evolution of influenza: drift or thrift? *Philos Trans R Soc Lond B Biol Sci*, 368(1614), 19 (2013).
9. Koel BF, van der Vliet S, Burke DF *et al.* Antigenic variation of clade 2.1 H5N1 virus is determined by a few amino acid substitutions immediately adjacent to the receptor binding site. *MBio*, 5(3), 01070-01014 (2014).
10. Krammer F, Smith GJD, Fouchier RAM *et al.* Influenza. *Nat Rev Dis Primers*, 4(1), 018-0002 (2018).
11. Kida H, Ito T, Yasuda J *et al.* Potential for transmission of avian influenza viruses to pigs. *J Gen Virol*, 75(Pt 9), 2183-2188 (1994).
12. Reid AH, Fanning TG, Hultin JV, Taubenberger JK. Origin and evolution of the 1918 "Spanish" influenza virus hemagglutinin gene. *Proc Natl Acad Sci U S A*, 96(4), 1651-1656 (1999).
13. Kawaoka Y, Krauss S, Webster RG. Avian-to-human transmission of the PB1 gene of influenza A viruses in the 1957 and 1968 pandemics. *J Virol*, 63(11), 4603-4608 (1989).
14. Nakajima K, Desselberger U, Palese P. Recent human influenza A (H1N1) viruses are closely related genetically to strains isolated in 1950. *Nature*, 274(5669), 334-339 (1978).
15. Schafer JR, Kawaoka Y, Bean WJ, Suss J, Senne D, Webster RG. Origin of the pandemic 1957 H2 influenza A virus and the persistence of its possible progenitors in the avian reservoir. *Virology*, 194(2), 781-788 (1993).
16. Organization WH. Pandemic influenza vaccine manufacturing process and timeline. (Ed.^(Eds)

17. Interim pre-pandemic planning guidance : community strategy for pandemic influenza mitigation in the United States : early, targeted, layered use of nonpharmaceutical interventions. (2007).
18. Qualls N, Levitt A, Kanade N *et al.* Community Mitigation Guidelines to Prevent Pandemic Influenza - United States, 2017. *MMWR. Recommendations and reports : Morbidity and mortality weekly report. Recommendations and reports*, 66(1), 1-34 (2017).
19. Bolton KJ, McCaw JM, Moss R *et al.* Likely effectiveness of pharmaceutical and non-pharmaceutical interventions for mitigating influenza virus transmission in Mongolia. *Bull World Health Organ*, 90(4), 264-271 (2012).
20. Cheng VCC, To KKW, Tse H, Hung IFN, Yuen K-Y. Two years after pandemic influenza A/2009/H1N1: what have we learned? *Clinical microbiology reviews*, 25(2), 223-263 (2012).
21. Update: drug susceptibility of swine-origin influenza A (H1N1) viruses, April 2009. *MMWR Morb Mortal Wkly Rep*, 58(16), 433-435 (2009).
22. Li IW, Hung IF, To KK *et al.* The natural viral load profile of patients with pandemic 2009 influenza A(H1N1) and the effect of oseltamivir treatment. *Chest*, 137(4), 759-768 (2010).
23. Ling LM, Chow AL, Lye DC *et al.* Effects of early oseltamivir therapy on viral shedding in 2009 pandemic influenza A (H1N1) virus infection. *Clin Infect Dis*, 50(7), 963-969 (2010).
24. Rewar S, Mirdha D, Rewar P. Treatment and Prevention of Pandemic H1N1 Influenza. *Ann Glob Health*, 81(5), 645-653 (2015).
25. Review of the 2010-2011 winter influenza season, northern hemisphere. *Wkly Epidemiol Rec*, 86(22), 222-227 (2011).
26. Inoue M, Barkham T, Leo YS *et al.* Emergence of oseltamivir-resistant pandemic (H1N1) 2009 virus within 48 hours. *Emerg Infect Dis*, 16(10), 1633-1636 (2010).
27. Paules C, Subbarao K. Influenza. *Lancet*, 390(10095), 697-708 (2017).
28. Skehel JJ, Bayley PM, Brown EB *et al.* Changes in the conformation of influenza virus hemagglutinin at the pH optimum of virus-mediated membrane fusion. *Proc Natl Acad Sci U S A*, 79(4), 968-972 (1982).
29. Pinto LH, Holsinger LJ, Lamb RA. Influenza virus M2 protein has ion channel activity. *Cell*, 69(3), 517-528 (1992).
30. White J, Matlin K, Helenius A. Cell fusion by Semliki Forest, influenza, and vesicular stomatitis viruses. *J Cell Biol*, 89(3), 674-679 (1981).
31. Martin K, Helenius A. Transport of incoming influenza virus nucleocapsids into the nucleus. *J Virol*, 65(1), 232-244 (1991).
32. Vreede FT, Jung TE, Brownlee GG. Model suggesting that replication of influenza virus is regulated by stabilization of replicative intermediates. *J Virol*, 78(17), 9568-9572 (2004).
33. Paterson D, Fodor E. Emerging roles for the influenza A virus nuclear export protein (NEP). *PLoS Pathog*, 8(12), 6 (2012).
34. Eisfeld AJ, Kawakami E, Watanabe T, Neumann G, Kawaoka Y. RAB11A is essential for transport of the influenza virus genome to the plasma membrane. *J Virol*, 85(13), 6117-6126 (2011).

35. Momose F, Kikuchi Y, Komase K, Morikawa Y. Visualization of microtubule-mediated transport of influenza viral progeny ribonucleoprotein. *Microbes Infect*, 9(12-13), 1422-1433 (2007).
36. Mora R, Rodriguez-Boulan E, Palese P, Garcia-Sastre A. Apical budding of a recombinant influenza A virus expressing a hemagglutinin protein with a basolateral localization signal. *J Virol*, 76(7), 3544-3553 (2002).
37. Barman S, Adhikary L, Chakrabarti AK, Bernas C, Kawaoka Y, Nayak DP. Role of transmembrane domain and cytoplasmic tail amino acid sequences of influenza a virus neuraminidase in raft association and virus budding. *J Virol*, 78(10), 5258-5269 (2004).
38. Nayak DP, Hui EK, Barman S. Assembly and budding of influenza virus. *Virus Res*, 106(2), 147-165 (2004).
39. Chen X, Liu S, Goraya MU, Maarouf M, Huang S, Chen J-L. Host Immune Response to Influenza A Virus Infection. *Frontiers in immunology*, 9, 320-320 (2018).
40. Rehwinkel J, Tan CP, Goubau D *et al.* RIG-I detects viral genomic RNA during negative-strand RNA virus infection. *Cell*, 140(3), 397-408 (2010).
41. Lund JM, Alexopoulou L, Sato A *et al.* Recognition of single-stranded RNA viruses by Toll-like receptor 7. *Proc Natl Acad Sci U S A*, 101(15), 5598-5603 (2004).
42. Ichinohe T, Lee HK, Ogura Y, Flavell R, Iwasaki A. Inflammasome recognition of influenza virus is essential for adaptive immune responses. *J Exp Med*, 206(1), 79-87 (2009).
43. Teijaro JR. The role of cytokine responses during influenza virus pathogenesis and potential therapeutic options. *Curr Top Microbiol Immunol*, 386, 3-22 (2015).
44. Garcia-Sastre A, Biron CA. Type 1 interferons and the virus-host relationship: a lesson in detente. *Science*, 312(5775), 879-882 (2006).
45. Gack MU, Shin YC, Joo CH *et al. TRIM25 RING-finger E3 ubiquitin ligase is essential for RIG-I-mediated antiviral activity* (Nature. 2007 Apr 19;446(7138):916-920. doi: 10.1038/nature05732.).
46. Wang X, Hinson ER, Cresswell P. The interferon-inducible protein viperin inhibits influenza virus release by perturbing lipid rafts. *Cell Host Microbe*, 2(2), 96-105 (2007).
47. Liu SY, Aliyari R, Chikere K *et al.* Interferon-inducible cholesterol-25-hydroxylase broadly inhibits viral entry by production of 25-hydroxycholesterol. *Immunity*, 38(1), 92-105 (2013).
48. Xiao H, Killip MJ, Staeheli P, Randall RE, Jackson D. The human interferon-induced MxA protein inhibits early stages of influenza A virus infection by retaining the incoming viral genome in the cytoplasm. *J Virol*, 87(23), 13053-13058 (2013).
49. Fu B, Wang L, Ding H, Schwamborn JC, Li S, Dorf ME. TRIM32 Senses and Restricts Influenza A Virus by Ubiquitination of PB1 Polymerase. *PLoS Pathog*, 11(6) (2015).
50. Tang Q, Wang X, Gao G. The Short Form of the Zinc Finger Antiviral Protein Inhibits Influenza A Virus Protein Expression and Is Antagonized by the Virus-Encoded NS1. *J Virol*, 91(2), 01909-01916 (2017).
51. Huber VC, Lynch JM, Bucher DJ, Le J, Metzger DW. Fc receptor-mediated phagocytosis makes a significant contribution to clearance of influenza virus infections. *J Immunol*, 166(12), 7381-7388 (2001).

52. Herold S, von Wulffen W, Steinmueller M *et al.* Alveolar epithelial cells direct monocyte transepithelial migration upon influenza virus infection: impact of chemokines and adhesion molecules. *J Immunol*, 177(3), 1817-1824 (2006).
53. Tate MD, Pickett DL, van Rooijen N, Brooks AG, Reading PC. Critical role of airway macrophages in modulating disease severity during influenza virus infection of mice. *Journal of virology*, 84(15), 7569-7580 (2010).
54. Mendelson M, Tekoah Y, Zilka A *et al.* NKp46 O-glycan sequences that are involved in the interaction with hemagglutinin type 1 of influenza virus. *J Virol*, 84(8), 3789-3797 (2010).
55. Ho AW, Prabhu N, Betts RJ *et al.* Lung CD103+ dendritic cells efficiently transport influenza virus to the lymph node and load viral antigen onto MHC class I for presentation to CD8 T cells. *J Immunol*, 187(11), 6011-6021 (2011).
56. Heer AK, Harris NL, Kopf M, Marsland BJ. CD4+ and CD8+ T cells exhibit differential requirements for CCR7-mediated antigen transport during influenza infection. *J Immunol*, 181(10), 6984-6994 (2008).
57. Whitmire JK, Tan JT, Whitton JL. Interferon-gamma acts directly on CD8+ T cells to increase their abundance during virus infection. *J Exp Med*, 201(7), 1053-1059 (2005).
58. Pipkin ME, Sacks JA, Cruz-Guilloty F, Lichtenheld MG, Bevan MJ, Rao A. Interleukin-2 and inflammation induce distinct transcriptional programs that promote the differentiation of effector cytolytic T cells. *Immunity*, 32(1), 79-90 (2010).
59. Topham DJ, Tripp RA, Doherty PC. CD8+ T cells clear influenza virus by perforin or Fas-dependent processes. *J Immunol*, 159(11), 5197-5200 (1997).
60. van Domselaar R, Bovenschen N. Cell death-independent functions of granzymes: hit viruses where it hurts. *Rev Med Virol*, 21(5), 301-314 (2011).
61. Brincks EL, Katewa A, Kucaba TA, Griffith TS, Legge KL. CD8 T cells utilize TRAIL to control influenza virus infection. *J Immunol*, 181(7), 4918-4925 (2008).
62. Stuber E, Strober W, Neurath M. Blocking the CD40L-CD40 interaction in vivo specifically prevents the priming of T helper 1 cells through the inhibition of interleukin 12 secretion. *J Exp Med*, 183(2), 693-698 (1996).
63. Teijaro JR, Verhoeven D, Page CA, Turner D, Farber DL. Memory CD4 T cells direct protective responses to influenza virus in the lungs through helper-independent mechanisms. *J Virol*, 84(18), 9217-9226 (2010).
64. Swain SL, McKinstry KK, Strutt TM. Expanding roles for $CD4^+$ T cells in immunity to viruses. *Nature reviews. Immunology*, 12(2), 136-148 (2012).
65. Schroder K, Hertzog PJ, Ravasi T, Hume DA. Interferon-gamma: an overview of signals, mechanisms and functions. *J Leukoc Biol*, 75(2), 163-189 (2004).
66. Cassatella MA, Bazzoni F, Flynn RM, Dusi S, Trinchieri G, Rossi F. Molecular basis of interferon-gamma and lipopolysaccharide enhancement of phagocyte respiratory burst capability. Studies on the gene expression of several NADPH oxidase components. *J Biol Chem*, 265(33), 20241-20246 (1990).
67. Karupiah G, Xie QW, Buller RM, Nathan C, Duarte C, MacMicking JD. Inhibition of viral replication by interferon-gamma-induced nitric oxide synthase. *Science*, 261(5127), 1445-1448 (1993).

68. Collier R. Revised WHO pandemic scale requires higher incidence of disease for most alert levels. *CMAJ : Canadian Medical Association journal = journal de l'Association medicale canadienne*, 180(12), E95-E96 (2009).
69. Fineberg HV. Pandemic preparedness and response--lessons from the H1N1 influenza of 2009. *N Engl J Med*, 370(14), 1335-1342 (2014).
70. Dawood FS, Iuliano AD, Reed C *et al.* Estimated global mortality associated with the first 12 months of 2009 pandemic influenza A H1N1 virus circulation: a modelling study. *Lancet Infect Dis*, 12(9), 687-695 (2012).
71. Canada PHAo. Lessons Learned Review: Public Health Agency of Canada and Health Canada Response to the 2009 H1N1 Pandemic. (Ed.^(Eds) (2010)
72. Information CIfH. The Impact of the H1N1 Pandemic on Canadian Hospitals. (Ed.^(Eds) (2010)
73. Van Kerkhove MD, Vandemaele KA, Shinde V *et al.* Risk factors for severe outcomes following 2009 influenza A (H1N1) infection: a global pooled analysis. *PLoS Med*, 8(7), 5 (2011).
74. McKenna JJ, Bramley AM, Skarbinski J, Fry AM, Finelli L, Jain S. Asthma in patients hospitalized with pandemic influenza A(H1N1)pdm09 virus infection-United States, 2009. *BMC Infect Dis*, 13(57), 1471-2334 (2013).
75. Dawood FS, Kamimoto L, D'Mello TA *et al.* Children with asthma hospitalized with seasonal or pandemic influenza, 2003-2009. *Pediatrics*, 128(1), 2010-3343 (2011).
76. Services UDoHaH. Summary Health Statistics for US Children: National Health Interview Survey. (Ed.^(Eds) (2009)
77. Organization WH. Global surveillance, prevention and control of chronic respiratory diseases. Khaltaev, JBaN (Ed.^(Eds) (Switzerland, 2007) 146.
78. Canada S. Asthma, 2014. (Ed.^(Eds) (2015)
79. Ismaila AS, Sayani AP, Marin M, Su Z. Clinical, economic, and humanistic burden of asthma in Canada: a systematic review. *BMC pulmonary medicine*, 13, 70-70 (2013).
80. Vital signs: asthma prevalence, disease characteristics, and self-management education: United States, 2001--2009. *MMWR Morb Mortal Wkly Rep*, 60(17), 547-552 (2011).
81. Nicolai T, Carr D, Weiland SK *et al.* Urban traffic and pollutant exposure related to respiratory outcomes and atopy in a large sample of children. *Eur Respir J*, 21(6), 956-963 (2003).
82. Strachan DP, Cook DG. Health effects of passive smoking. 6. Parental smoking and childhood asthma: longitudinal and case-control studies. *Thorax*, 53(3), 204-212 (1998).
83. Szabo SM, Levy AR, Gooch KL, Bradt P, Wijaya H, Mitchell I. Elevated risk of asthma after hospitalization for respiratory syncytial virus infection in infancy. *Paediatr Respir Rev*, 13(2), 70161-70166 (2013).
84. Okada H, Kuhn C, Feillet H, Bach JF. The 'hygiene hypothesis' for autoimmune and allergic diseases: an update. *Clin Exp Immunol*, 160(1), 1-9 (2010).
85. Ege MJ, Mayer M, Normand AC *et al.* Exposure to environmental microorganisms and childhood asthma. *N Engl J Med*, 364(8), 701-709 (2011).
86. Kausel L, Boneberger A, Calvo M, Radon K. Childhood asthma and allergies in urban, semiurban, and rural residential sectors in Chile. *ScientificWorldJournal*, 23(937935) (2013).

87. Weinberg EG. Urbanization and childhood asthma: an African perspective. *J Allergy Clin Immunol*, 105(2 Pt 1), 224-231 (2000).
88. Backman H, Raisanen P, Hedman L *et al.* Increased prevalence of allergic asthma from 1996 to 2006 and further to 2016-results from three population surveys. *Clin Exp Allergy*, 47(11), 1426-1435 (2017).
89. Wenzel SE. Asthma phenotypes: the evolution from clinical to molecular approaches. *Nat Med*, 18(5), 716-725 (2012).
90. Al-Ramli W, Prefontaine D, Chouiali F *et al. T(H)17-associated cytokines (IL-17A and IL-17F) in severe asthma* (J Allergy Clin Immunol. 2009 May;123(5):1185-7. doi: 10.1016/j.jaci.2009.02.024. Epub 2009 Apr 10.).
91. Chakir J, Shannon J, Molet S *et al.* Airway remodeling-associated mediators in moderate to severe asthma: effect of steroids on TGF-beta, IL-11, IL-17, and type I and type III collagen expression. *J Allergy Clin Immunol*, 111(6), 1293-1298 (2003).
92. Levy ML, Fletcher M, Price DB, Hausen T, Halbert RJ, Yawn BP. International Primary Care Respiratory Group (IPCRG) Guidelines: diagnosis of respiratory diseases in primary care. *Prim Care Respir J*, 15(1), 20-34 (2006).
93. Celli BR. The importance of spirometry in COPD and asthma: effect on approach to management. *Chest*, 117(2 Suppl), 15S-19S (2000).
94. Nair P, Martin JG, Cockcroft DC *et al.* Airway Hyperresponsiveness in Asthma: Measurement and Clinical Relevance. *J Allergy Clin Immunol Pract*, 5(3), 649-659 (2017).
95. Jones SL, Kittelson J, Cowan JO *et al.* The predictive value of exhaled nitric oxide measurements in assessing changes in asthma control. *Am J Respir Crit Care Med*, 164(5), 738-743 (2001).
96. Sandeep T, Roopakala MS, Silvia CRWD, Chandrashekara S, Rao M. Evaluation of serum immunoglobulin E levels in bronchial asthma. *Lung India : official organ of Indian Chest Society*, 27(3), 138-140 (2010).
97. Lee SE, Jeong SK, Lee SH. Protease and protease-activated receptor-2 signaling in the pathogenesis of atopic dermatitis. *Yonsei Med J*, 51(6), 808-822 (2010).
98. Tomee JF, van Weissenbruch R, de Monchy JG, Kauffman HF. Interactions between inhalant allergen extracts and airway epithelial cells: effect on cytokine production and cell detachment. *J Allergy Clin Immunol*, 102(1), 75-85 (1998).
99. Yu HS, Angkasekwinai P, Chang SH, Chung Y, Dong C. Protease allergens induce the expression of IL-25 via Erk and p38 MAPK pathway. *J Korean Med Sci*, 25(6), 829-834 (2010).
100. Kamijo S, Takeda H, Tokura T *et al.* IL-33-mediated innate response and adaptive immune cells contribute to maximum responses of protease allergen-induced allergic airway inflammation. *J Immunol*, 190(9), 4489-4499 (2013).
101. Wan H, Winton HL, Soeller C *et al.* Quantitative structural and biochemical analyses of tight junction dynamics following exposure of epithelial cells to house dust mite allergen Der p 1. *Clin Exp Allergy*, 30(5), 685-698 (2000).
102. Pichavant M, Charbonnier AS, Taront S *et al.* Asthmatic bronchial epithelium activated by the proteolytic allergen Der p 1 increases selective dendritic cell recruitment. *J Allergy Clin Immunol*, 115(4), 771-778 (2005).

103. Deslee G, Charbonnier AS, Hammad H *et al.* Involvement of the mannose receptor in the uptake of Der p 1, a major mite allergen, by human dendritic cells. *J Allergy Clin Immunol*, 110(5), 763-770 (2002).
104. Taylor PR, Gordon S, Martinez-Pomares L. The mannose receptor: linking homeostasis and immunity through sugar recognition. *Trends Immunol*, 26(2), 104-110 (2005).
105. Kayserova J, Zentsova-Jaresova I, Budinsky V *et al.* Selective increase in blood dendritic cell antigen-3-positive dendritic cells in bronchoalveolar lavage fluid in allergic patients. *Scand J Immunol*, 75(3), 305-313 (2012).
106. Royer PJ, Emara M, Yang C *et al.* The mannose receptor mediates the uptake of diverse native allergens by dendritic cells and determines allergen-induced T cell polarization through modulation of IDO activity. *J Immunol*, 185(3), 1522-1531 (2010).
107. Chiou YL, Lin CY. Der p2 activates airway smooth muscle cells in a TLR2/MyD88-dependent manner to induce an inflammatory response. *J Cell Physiol*, 220(2), 311-318 (2009).
108. Trompette A, Divanovic S, Visintin A *et al.* Allergenicity resulting from functional mimicry of a Toll-like receptor complex protein. *Nature*, 457(7229), 585-588 (2009).
109. Ito T, Wang YH, Duramad O *et al.* TSLP-activated dendritic cells induce an inflammatory T helper type 2 cell response through OX40 ligand. *J Exp Med*, 202(9), 1213-1223 (2005).
110. Prefontaine D, Nadigel J, Chouiali F *et al. Increased IL-33 expression by epithelial cells in bronchial asthma* (J Allergy Clin Immunol. 2010 Mar;125(3):752-4. doi: 10.1016/j.jaci.2009.12.935. Epub 2010 Feb 11.).
111. Beale J, Jayaraman A, Jackson DJ *et al.* Rhinovirus-induced IL-25 in asthma exacerbation drives type 2 immunity and allergic pulmonary inflammation. *Sci Transl Med*, 6(256), 3009124 (2014).
112. Bartemes KR, Iijima K, Kobayashi T, Kephart GM, McKenzie AN, Kita H. IL-33-responsive lineage- CD25+ CD44(hi) lymphoid cells mediate innate type 2 immunity and allergic inflammation in the lungs. *J Immunol*, 188(3), 1503-1513 (2012).
113. Kurowska-Stolarska M, Kewin P, Murphy G *et al.* IL-33 induces antigen-specific IL-5+ T cells and promotes allergic-induced airway inflammation independent of IL-4. *J Immunol*, 181(7), 4780-4790 (2008).
114. Schmitz J, Owyang A, Oldham E *et al.* IL-33, an interleukin-1-like cytokine that signals via the IL-1 receptor-related protein ST2 and induces T helper type 2-associated cytokines. *Immunity*, 23(5), 479-490 (2005).
115. Angkasekwinai P, Park H, Wang YH *et al.* Interleukin 25 promotes the initiation of proallergic type 2 responses. *J Exp Med*, 204(7), 1509-1517 (2007).
116. Neill DR, Wong SH, Bellosi A *et al.* Nuocytes represent a new innate effector leukocyte that mediates type-2 immunity. *Nature*, 464(7293), 1367-1370 (2010).
117. Pease JE, Williams TJ. Eotaxin and asthma. *Curr Opin Pharmacol*, 1(3), 248-253 (2001).
118. Hirst SJ, Hallsworth MP, Peng Q, Lee TH. Selective Induction of Eotaxin Release by Interleukin-13 or Interleukin-4 in Human Airway Smooth Muscle Cells Is Synergistic with Interleukin-1 β and Is Mediated by the Interleukin-4 Receptor α -Chain. *American Journal of Respiratory and Critical Care Medicine*, 165(8), 1161-1171 (2002).

119. Kuo HP, Wang CH, Lin HC, Hwang KS, Liu SL, Chung KF. Interleukin-5 in growth and differentiation of blood eosinophil progenitors in asthma: effect of glucocorticoids. *British journal of pharmacology*, 134(7), 1539-1547 (2001).
120. James AL, Wenzel S. Clinical relevance of airway remodelling in airway diseases. *Eur Respir J*, 30(1), 134-155 (2007).
121. Zuyderduyn S, Ninaber DK, Schrumpf JA *et al.* IL-4 and IL-13 exposure during mucociliary differentiation of bronchial epithelial cells increases antimicrobial activity and expression of antimicrobial peptides. *Respir Res*, 12(59), 1465-9921 (2011).
122. Tyner JW, Kim EY, Ide K *et al.* Blocking airway mucous cell metaplasia by inhibiting EGFR antiapoptosis and IL-13 transdifferentiation signals. *J Clin Invest*, 116(2), 309-321 (2006).
123. Park KS, Korfhagen TR, Bruno MD *et al.* SPDEF regulates goblet cell hyperplasia in the airway epithelium. *J Clin Invest*, 117(4), 978-988 (2007).
124. O'Reilly S, Ciechomska M, Fullard N, Przyborski S, van Laar JM. IL-13 mediates collagen deposition via STAT6 and microRNA-135b: a role for epigenetics. *Scientific reports*, 6, 25066-25066 (2016).
125. Mosmann TR, Cherwinski H, Bond MW, Giedlin MA, Coffman RL. Two types of murine helper T cell clone. I. Definition according to profiles of lymphokine activities and secreted proteins. *J Immunol*, 136(7), 2348-2357 (1986).
126. Evans CM, Jenner RG. Transcription factor interplay in T helper cell differentiation. *Briefings in functional genomics*, 12(6), 499-511 (2013).
127. Daines MO, Hershey GK. A novel mechanism by which interferon-gamma can regulate interleukin (IL)-13 responses. Evidence for intracellular stores of IL-13 receptor alpha -2 and their rapid mobilization by interferon-gamma. *J Biol Chem*, 277(12), 10387-10393 (2002).
128. Hwang ES, Szabo SJ, Schwartzberg PL, Glimcher LH. T helper cell fate specified by kinase-mediated interaction of T-bet with GATA-3. *Science*, 307(5708), 430-433 (2005).
129. Usui T, Nishikomori R, Kitani A, Strober W. GATA-3 suppresses Th1 development by downregulation of Stat4 and not through effects on IL-12Rbeta2 chain or T-bet. *Immunity*, 18(3), 415-428 (2003).
130. Conrad ML, Yildirim AO, Sonar SS *et al.* Comparison of adjuvant and adjuvant-free murine experimental asthma models. *Clin Exp Allergy*, 39(8), 1246-1254 (2009).
131. Sagar S, Akbarshahi H, Uller L. Translational value of animal models of asthma: Challenges and promises. *Eur J Pharmacol*, 759, 272-277 (2015).
132. Jungsuwadee P, Benkovszky M, Dekan G, Stingl G, Epstein MM. Repeated aerosol allergen exposure suppresses inflammation in B-cell-deficient mice with established allergic asthma. *Int Arch Allergy Immunol*, 133(1), 40-48 (2004).
133. Chang YS, Kim YK, Bahn JW *et al.* Comparison of asthma phenotypes using different sensitizing protocols in mice. *Korean J Intern Med*, 20(2), 152-158 (2005).
134. Hatzivlassiou M, Grainge C, Kehagia V, Lau L, Howarth PH. The allergen specificity of the late asthmatic reaction. *Allergy*, 65(3), 355-358 (2010).
135. Johnson JR, Wiley RE, Fattouh R *et al.* Continuous exposure to house dust mite elicits chronic airway inflammation and structural remodeling. *Am J Respir Crit Care Med*, 169(3), 378-385 (2004).

136. Hammad H, Chieppa M, Perros F, Willart MA, Germain RN, Lambrecht BN. House dust mite allergen induces asthma via Toll-like receptor 4 triggering of airway structural cells. *Nat Med*, 15(4), 410-416 (2009).
137. Gregory LG, Causton B, Murdoch JR *et al.* Inhaled house dust mite induces pulmonary T helper 2 cytokine production. *Clin Exp Allergy*, 39(10), 1597-1610 (2009).
138. Kim HS, Lee H, Kim HS *et al.* Effect of Influenza Virus Infection in a Murine Model of Asthma. *Iran J Allergy Asthma Immunol*, 14(4), 392-401 (2015).
139. Mahmutovic Persson I, Akbarshahi H, Menzel M, Brandelius A, Uller L. Increased expression of upstream TH2-cytokines in a mouse model of viral-induced asthma exacerbation. *J Transl Med*, 14(52), 016-0808 (2016).
140. Phan JA, Kicic A, Berry LJ *et al.* Rhinovirus exacerbates house-dust-mite induced lung disease in adult mice. *PLoS One*, 9(3) (2014).
141. Ravanetti L, Dijkhuis A, Sabogal Pineros YS *et al.* An early innate response underlies severe influenza-induced exacerbations of asthma in a novel steroid-insensitive and anti-IL-5-responsive mouse model. *Allergy*, 72(5), 737-753 (2017).
142. Gavett SH, O'Hearn DJ, Karp CL *et al.* Interleukin-4 receptor blockade prevents airway responses induced by antigen challenge in mice. *Am J Physiol*, 272(2 Pt 1) (1997).
143. Hirota JA. Airway Remodelling in Mouse Models of Exposure to Allergen. In: *Physiology and Pharmacology.* (Ed.^(Eds) (McMaster University, Hamilton, Canada, 2009) 265.
144. Royce SG, Patel KP, Samuel CS. Characterization of a novel model incorporating airway epithelial damage and related fibrosis to the pathogenesis of asthma. *Lab Invest*, 94(12), 1326-1339 (2014).
145. Fouchier RA, Bestebroer TM, Herfst S, Van Der Kemp L, Rimmelzwaan GF, Osterhaus AD. Detection of influenza A viruses from different species by PCR amplification of conserved sequences in the matrix gene. *J Clin Microbiol*, 38(11), 4096-4101 (2000).
146. Southam DS, Ellis R, Wattie J, Inman MD. Components of airway hyperresponsiveness and their associations with inflammation and remodeling in mice. *J Allergy Clin Immunol*, 119(4), 848-854 (2007).
147. Woo LN, Guo WY, Wang X *et al.* A 4-Week Model of House Dust Mite (HDM) Induced Allergic Airways Inflammation with Airway Remodeling. *Sci Rep*, 8(1), 018-24574 (2018).
148. Phipps S, Lam CE, Mahalingam S *et al.* Eosinophils contribute to innate antiviral immunity and promote clearance of respiratory syncytial virus. *Blood*, 110(5), 1578-1586 (2007).
149. Piyadasa H, Altieri A, Basu S, Schwartz J, Halayko AJ, Mookherjee N. Biosignature for airway inflammation in a house dust mite-challenged murine model of allergic asthma. *Biol Open*, 5(2), 112-121 (2016).
150. Wark PA, Johnston SL, Bucchieri F *et al.* Asthmatic bronchial epithelial cells have a deficient innate immune response to infection with rhinovirus. *J Exp Med*, 201(6), 937-947 (2005).
151. Raundhal M, Morse C, Khare A *et al.* High IFN-gamma and low SLPI mark severe asthma in mice and humans. *J Clin Invest*, 125(8), 3037-3050 (2015).

152. Kumar RK, Yang M, Herbert C, Foster PS. Interferon-gamma, pulmonary macrophages and airway responsiveness in asthma. *Inflamm Allergy Drug Targets*, 11(4), 292-297 (2012).
153. Mitchell C, Provost K, Niu N, Homer R, Cohn L. IFN-gamma acts on the airway epithelium to inhibit local and systemic pathology in allergic airway disease. *J Immunol*, 187(7), 3815-3820 (2011).
154. Message SD, Laza-Stanca V, Mallia P *et al.* Rhinovirus-induced lower respiratory illness is increased in asthma and related to virus load and Th1/2 cytokine and IL-10 production. *Proc Natl Acad Sci U S A*, 105(36), 13562-13567 (2008).
155. Robinson DS, Hamid Q, Ying S *et al.* Predominant TH2-like bronchoalveolar T-lymphocyte population in atopic asthma. *N Engl J Med*, 326(5), 298-304 (1992).
156. Moussion C, Ortega N, Girard JP. The IL-1-like cytokine IL-33 is constitutively expressed in the nucleus of endothelial cells and epithelial cells in vivo: a novel 'alarmin'? *PLoS One*, 3(10), 0003331 (2008).
157. Mjosberg JM, Trifari S, Crellin NK *et al.* Human IL-25- and IL-33-responsive type 2 innate lymphoid cells are defined by expression of CRTH2 and CD161. *Nat Immunol*, 12(11), 1055-1062 (2011).
158. Jackson DJ, Makrinioti H, Rana BM *et al.* IL-33-dependent type 2 inflammation during rhinovirus-induced asthma exacerbations in vivo. *Am J Respir Crit Care Med*, 190(12), 1373-1382 (2014).
159. Borish LC, Nelson HS, Lanz MJ *et al.* Interleukin-4 receptor in moderate atopic asthma. A phase I/II randomized, placebo-controlled trial. *Am J Respir Crit Care Med*, 160(6), 1816-1823 (1999).
160. Borish LC, Nelson HS, Corren J *et al.* Efficacy of soluble IL-4 receptor for the treatment of adults with asthma. *J Allergy Clin Immunol*, 107(6), 963-970 (2001).
161. Zeskind B. *Lebrikizumab treatment in adults with asthma* (N Engl J Med. 2011 Dec 22;365(25):2432; author reply 2433-4. doi: 10.1056/NEJMc1112234.).
162. Scheerens H, Arron JR, Zheng Y *et al.* The effects of lebrikizumab in patients with mild asthma following whole lung allergen challenge. *Clin Exp Allergy*, 44(1), 38-46 (2014).
163. Fala L. Nucala (Mepolizumab): First IL-5 Antagonist Monoclonal Antibody FDA Approved for Maintenance Treatment of Patients with Severe Asthma. *American health & drug benefits*, 9(Spec Feature), 106-110 (2016).
164. Ortega HG, Liu MC, Pavord ID *et al.* Mepolizumab treatment in patients with severe eosinophilic asthma. *N Engl J Med*, 371(13), 1198-1207 (2014).
165. Reinke T. Dupixent, a New Entrant In the Asthma Lists. *Manag Care*, 27(9), 14 (2018).
166. Busse WW, Maspero JF, Rabe KF *et al.* Liberty Asthma QUEST: Phase 3 Randomized, Double-Blind, Placebo-Controlled, Parallel-Group Study to Evaluate Dupilumab Efficacy/Safety in Patients with Uncontrolled, Moderate-to-Severe Asthma. *Adv Ther*, 3(10), 018-0702 (2018).
167. Rabe KF, Nair P, Brusselle G *et al.* Efficacy and Safety of Dupilumab in Glucocorticoid-Dependent Severe Asthma. *N Engl J Med*, 378(26), 2475-2485 (2018).
168. Wenzel S, Ford L, Pearlman D *et al.* Dupilumab in persistent asthma with elevated eosinophil levels. *N Engl J Med*, 368(26), 2455-2466 (2013).

169. Hirota JA, Budelsky A, Smith D *et al.* The role of interleukin-4Ralpha in the induction of glutamic acid decarboxylase in airway epithelium following acute house dust mite exposure. *Clin Exp Allergy*, 40(5), 820-830 (2010).
170. Aman MJ, Tayebi N, Obiri NI, Puri RK, Modi WS, Leonard WJ. cDNA cloning and characterization of the human interleukin 13 receptor alpha chain. *J Biol Chem*, 271(46), 29265-29270 (1996).
171. Donaldson DD, Whitters MJ, Fitz LJ *et al.* The murine IL-13 receptor alpha 2: molecular cloning, characterization, and comparison with murine IL-13 receptor alpha 1. *J Immunol*, 161(5), 2317-2324 (1998).
172. LaPorte SL, Juo ZS, Vaclavikova J *et al.* Molecular and structural basis of cytokine receptor pleiotropy in the interleukin-4/13 system. *Cell*, 132(2), 259-272 (2008).
173. Kelly-Welch AE, Hanson EM, Boothby MR, Keegan AD. Interleukin-4 and interleukin-13 signaling connections maps. *Science*, 300(5625), 1527-1528 (2003).
174. Mikita T, Campbell D, Wu P, Williamson K, Schindler U. Requirements for interleukin-4-induced gene expression and functional characterization of Stat6. *Mol Cell Biol*, 16(10), 5811-5820 (1996).
175. Heller NM, Qi X, Junttila IS *et al.* Type I IL-4Rs selectively activate IRS-2 to induce target gene expression in macrophages. *Sci Signal*, 1(51), 1164795 (2008).
176. Carey GB, Semenova E, Qi X, Keegan AD. IL-4 protects the B-cell lymphoma cell line CH31 from anti-IgM-induced growth arrest and apoptosis: contribution of the PI-3 kinase/AKT pathway. *Cell Res*, 17(11), 942-955 (2007).
177. Tliba O, Deshpande D, Chen H *et al.* IL-13 enhances agonist-evoked calcium signals and contractile responses in airway smooth muscle. *Br J Pharmacol*, 140(7), 1159-1162 (2003).
178. Wijesundara DK, Tscharke DC, Jackson RJ, Ranasinghe C. Reduced interleukin-4 receptor alpha expression on CD8+ T cells correlates with higher quality anti-viral immunity. *PLoS One*, 8(1), 31 (2013).
179. Contoli M, Ito K, Padovani A *et al.* Th2 cytokines impair innate immune responses to rhinovirus in respiratory epithelial cells. *Allergy*, 70(8), 910-920 (2015).
180. Lu M, Dawicki W, Zhang X, Huang H, Nayyar A, Gordon JR. Therapeutic induction of tolerance by IL-10-differentiated dendritic cells in a mouse model of house dust mite-asthma. *Allergy*, 66(5), 612-620 (2011).
181. Tomkinson A, Duez C, Cieslewicz G *et al.* A murine IL-4 receptor antagonist that inhibits IL-4- and IL-13-induced responses prevents antigen-induced airway eosinophilia and airway hyperresponsiveness. *J Immunol*, 166(9), 5792-5800 (2001).
182. Doe C, Bafadhel M, Siddiqui S *et al.* Expression of the T helper 17-associated cytokines IL-17A and IL-17F in asthma and COPD. *Chest*, 138(5), 1140-1147 (2010).
183. Molet S, Hamid Q, Davoine F *et al.* IL-17 is increased in asthmatic airways and induces human bronchial fibroblasts to produce cytokines. *J Allergy Clin Immunol*, 108(3), 430-438 (2001).
184. Zhou QT, Sun YC, Yao WZ. [Characteristics of the airway inflammation and the relationship to interleukin-17 in severe asthma]. *Zhonghua Jie He He Hu Xi Za Zhi*, 28(9), 630-634 (2005).

185. Newcomb DC, Boswell MG, Sherrill TP *et al.* IL-17A induces signal transducers and activators of transcription-6-independent airway mucous cell metaplasia. *Am J Respir Cell Mol Biol*, 48(6), 711-716 (2013).
186. Ripple MJ, You D, Honnegowda S *et al.* Immunomodulation with IL-4R alpha antisense oligonucleotide prevents respiratory syncytial virus-mediated pulmonary disease. *J Immunol*, 185(8), 4804-4811 (2010).
187. Organization WH. Report of the WHO pandemic influenza A(H1N1) vaccine deployment initiative. (Ed.^(Eds) (Geneva)
188. Prevention CfDCa. Age Group Distribution of Influenza Positive Specimens Reported by Public Health Laboratories, National Summary. (Ed.^(Eds) (2018)
189. Organization WH. Support for developing countries' response to the H1N1 influenza pandemic. (Ed.^(Eds) (2009)
190. Birrell MA, Van Oosterhout AJ, Belvisi MG. *Do the current house dust mite-driven models really mimic allergic asthma?* (Eur Respir J. 2010 Nov;36(5):1220-1. doi: 10.1183/09031936.00069110.).
191. Kasaian MT, Marquette K, Fish S *et al.* An IL-4/IL-13 dual antagonist reduces lung inflammation, airway hyperresponsiveness, and IgE production in mice. *Am J Respir Cell Mol Biol*, 49(1), 37-46 (2013).
192. Walford HH, Doherty TA. STAT6 and lung inflammation. *JAK-STAT*, 2(4), e25301-e25301 (2013).
193. Heller NM, Qi X, Junttila IS *et al.* Type I IL-4Rs selectively activate IRS-2 to induce target gene expression in macrophages. *Science signaling*, 1(51), ra17-ra17 (2008).
194. Wills-Karp M, Finkelman FD. Untangling the complex web of IL-4- and IL-13-mediated signaling pathways. *Sci Signal*, 1(51) (2008).
195. Wurster AL, Withers DJ, Uchida T, White MF, Grusby MJ. Stat6 and IRS-2 cooperate in interleukin 4 (IL-4)-induced proliferation and differentiation but are dispensable for IL-4-dependent rescue from apoptosis. *Mol Cell Biol*, 22(1), 117-126 (2002).
196. Gern JE. How rhinovirus infections cause exacerbations of asthma. *Clin Exp Allergy*, 45(1), 32-42 (2015).
197. Kim WK. Association between respiratory viruses and asthma exacerbations. *Korean journal of pediatrics*, 57(1), 26-28 (2014).
198. Gao R, Cao B, Hu Y *et al.* Human infection with a novel avian-origin influenza A (H7N9) virus. *N Engl J Med*, 368(20), 1888-1897 (2013).
199. Zhou L, Tan Y, Kang M *et al.* Preliminary Epidemiology of Human Infections with Highly Pathogenic Avian Influenza A(H7N9) Virus, China, 2017. *Emerging infectious diseases*, 23(8), 1355-1359 (2017).
200. Hai R, Schmolke M, Leyva-Grado VH *et al.* Influenza A(H7N9) virus gains neuraminidase inhibitor resistance without loss of in vivo virulence or transmissibility. *Nat Commun*, 4(2854) (2013).
201. Hay AJ, Hayden FG. Oseltamivir resistance during treatment of H7N9 infection. *Lancet*, 381(9885), 2230-2232 (2013).